UNIVERSITY OF CALIFORNIA
SANTA CRUZ

MONTE CARLO STUDIES OF DISORDERED SPIN SYSTEMS

A dissertation submitted in partial satisfaction of the
requirements for the degree of

DOCTOR OF PHILOSOPHY

in

PHYSICS

by

Derek A. Larson

June 2009

The Dissertation of Derek A. Larson
is approved:

Professor A. Peter Young, Chair

Professor David Belanger

Professor Josh Deutsch

Dean Lisa C. Sloan
Vice Provost and Dean of Graduate Studies

Copyright © by

Derek A. Larson

2009

Table of Contents

List of Figures

List of Tables

Abstract

Monte Carlo studies of disordered spin systems

by

Derek A. Larson

We present our findings on four topics relating to disordered spin systems. The first is on a technique to optimize Monte Carlo simulations. This technique was successfully applied to simple models, such as the Ising ferromagnet, in earlier published work. We explore its application to a basic spin glass model and find it of limited use. Put simply, spin glasses are too different qualitatively from the systems for which the optimization was shown to be effective.

The second topic concerns the debate over the existence of the Almeida-Thouless (AT) line *i.e.* whether or not Ising spin glasses have a transition in a field. We study an Ising spin glass on a one-dimensional model which has interactions that decay as a power of distance; tuning this power allows us to modify the effective range of the system. The analysis is based on a finite-size scaling of the dimensionless correlation length, which we use to find evidence for second-order transitions. Our results suggest that an AT line exists for dimensions greater than six and does not exist for lower dimensions. The data shown are from simulations by Katzgraber, while Larson checked select results with independent source code to ensure their validity. All collaborators contributed to the analysis of these data.

Third, we investigate a "p-spin" spin glass, for $p = 3$, motivated by analogies to structural glass physics as well as an argument that it belongs in the same universality class as the Ising model in a field. Specifically, there is a strong connection between the mean field dynamics of this model and the Mode Coupling Theory of structural glasses. The goal is to see if the mean field description carries to low dimensionsality. We use a similar one-dimensional model to the above in order to probe multiple dimensions for phase transitions. We again look for evidence in the correlation length. The findings indicate transitions both above and below a dimension of six, though the transition disappears for sufficiently low dimension (above d_l). We discuss possible sources for the different behavior between the 3-spin model and the Ising glass in a field.

In the last topic we look for evidence of the Griffiths singularity in a bond-diluted two-dimensional XY ferromagnet. The Griffiths singularity should appear (weakly) in the tail of the susceptibility distribution for different bond realizations. We apply a powerful distribution-sampling technique to this end. Our results suggest that the susceptibility distribution does indeed respond to the singularity, though not as cleanly as in a similar study on the Ising model. The weaker form of ordering for XY models may be the cause of this.

To The Future,

may it be merciful,

Acknowledgments

I owe my graduate career to Peter Young, at once both a top theorist in his field and a sagely mentor to his students. Through him I believe I have found a calling to which I can dedicate myself. Many thanks are due for Helmut Katzgraber, collaborator and source of (computational) muscle. As a less-crystallized professor, he has provided a more realistic template for my continuing academic career (not to mention providing for a lovely visit to Switzerland to collaborate at ETH Zurich). A thank you to David Doshay and the Hierarchical Systems Research Foundation provided considerable computer time for my projects. Dave Belanger and Josh Deutsch deserve credit for their role on my reading committee, and have earned my gratitude for their occasional assistance throughout my time here. Also to Luke Winstrom and Jeff Jones: we began together and we ended together. Thanks for the good times.

I give special thanks to my parents, my support from afar, and to Elsie Tanadjaja, my support at home.

The text of this dissertation includess reprints of the following previously published material:

- *Study of the Almeida-Thouless line using power-law diluted one-dimensional Ising spin glasses*, H. G. Katzgraber, D. Larson, and A. P. Young, Phys. Rev. Lett. **102**, 177205 (2009).

Chapter 1

Introduction to Disordered Systems

The simplest systems to ponder are those with the highest symmetry. As one expects, these systems tend to be the first to be understood. Thus, modern physics is increasingly interested in the effects of *disorder*, which is ultimately a mechanism for breaking symmetries. Without these symmetries, theoretical descriptions become more cumbersome and finding analytic solutions may prove impossible. The increasing difficulty of exact theoretical analysis of disordered systems has led physicists to other methods of arriving at answers, namely numerical methods. With the advent of the computer, large-scale numerical calculations became feasible, and with the developments in semiconductors over the decades, numerical simulations have now become the dominant investigative technique for many areas of physics.

Disorder in nature falls into two broad categories: quenched and annealed. Quenched disorder can be described as "fixed"– on experimental time scales and for changing temperatures, it remains constant. Conversely, annealed disorder is that which

may change as the system evolves. This chapter discusses two types of disordered systems involving quenched disorder, spin glasses and structural glasses, which have interesting similarities that are explored in this work.

1.1 Interacting Spins

Before attacking disordered systems like spin glasses, it is important to first understand the pure systems upon which they are based. This thesis is concerned with how "spins", generally atomic magnetic moments, interact. The simplest such is a one-dimensional "chain" of spins where each interacts with its two neighbors, and each pair prefers to point in the same direction–a *ferromagnetic* interaction. Then, if we constrain the spins to be collinear, so each spin only has two states "up" and "down", we arrive at the model that Ernst Ising first solved in 1925–perhaps the foundation of the study of spin systems. The Hamiltonian can be written,

$$\mathcal{H} = -J \sum_{\langle i,j \rangle} S_i S_j \tag{1.1}$$

where the $S_i = \pm 1$, J is the interaction strength, and $\langle i, j \rangle$ implies summation over nearest neighbors only. For such a model, one of the first questions would be whether or not it has a phase transition separating an ordered, low temperature state from a disordered, high temperature one. Such a transition would be characterized by an *order parameter*, which for a ferromagnetic system is simply $m = \frac{1}{N} \sum_i S_i$, the magnetization per spin (where N is the number of spins). Ising showed that the model does not exhibit such a phase transition at non-zero temperature [32]. However, 19 years later,

Lars Onsager found a remarkable solution [61] to the two-dimensional version of the same model, where the spins are laid out on a square lattice. It *does* feature a phase transition at a critical temperature $T_c = \frac{2}{\ln(1+\sqrt{2})}$. Crossing this transition from high temperature to low temperature, one would see m begin to continuously deviate from zero at T_c, indicating an onset of order. Another observable that would respond to the transition is the magnetic susceptibility,

$$\chi = (\frac{dm}{dh})|_{h=0} \tag{1.2}$$

which *diverges* at T_c. A susceptibility is generally a measure of how an order parameter responds to changes in the related field; in this case the change in magnetization with applied magnetic field. At the critical temperature, the system is primed for spontaneous ordering without this symmetry-breaking field, thus applying an infinitesimal amount would yield a large response, hence the divergence.

1.2 Spin Glasses

The concept of a spin glass can be explained by considering a simple experimental system that contains all of the necessary ingredients. One such is gold doped with iron, Fe_xAu_{1-x}. Gold forms a non-magnetic bulk in which the magnetic iron impurities interact with each other. This type of interaction was successfully described by Ruderman, Kittel, Kasuya, and Yosida (RKKY) and involves a coupling between the nuclear and core electron spins between two sites mediated by the bulk conduction

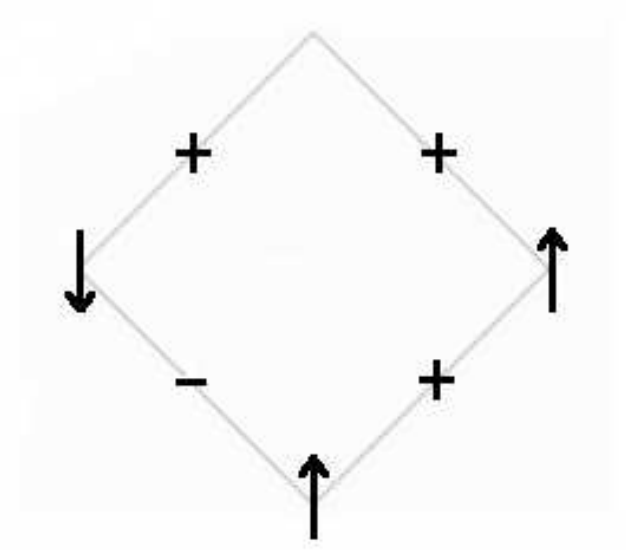

Figure 1.1: An example of frustration: a spin placed at the top of the diamond will be under competing influences from its two neighbors. It cannot simultaneously satisfy both.

electrons. It takes the form,

$$J(r) = J_0 \frac{\cos(2rk_F)}{(rk_F)^3} \tag{1.3}$$

where k_F is the Fermi momentum, and is notable for the r-dependent oscillations in sign. Since the iron atoms are inserted randomly into the lattice, their distance from each other, and hence the sign of the interaction, will be random. This is an example of quenched disorder (the iron atoms diffuse slowly on experimental time scales), and it may lead to a situation depicted in Fig.(1.1). This is called *frustration*. In this case, a spin located at the vacant site is told to align to both of its neighbors which point in opposite directions. If the strengths of the interactions are equivalent, a ground state

degeneracy will exist. This disorder-induced frustration is the key feature of the spin glass.

By introducing disorder to the Ising model, we can write down a basic spin glass model called the Edwards-Anderson (EA) glass [15],

$$\mathcal{H} = -\sum_{\langle i,j \rangle} J_{ij} S_i S_j \tag{1.4}$$

where J_{ij} are now random variables symmetric about 0, and the S_i are still Ising spins ($S_i = \pm 1$). These interactions mimic the nature of the RKKY interactions by having random sign. The standard convention is to place the spins on a *hyper*cubic lattice where each spin has $2d$ nearest neighbors in d dimensions. While this is a highly symmetric arrangement that won't geometrically match a system like FeAu at all, also randomizing the magnitude of the interaction strength, in addition to the sign, recaptures elements of the random distance between sites. Again, now that we have a model, one of the first properties to explore is the ordering behavior. It is straightforward to show analytically that the system *cannot* (anti)ferromagnetically order due to the symmetry of the interactions. However, a subtler form of order exists.

Early experiments performed on Fe_xAu_{1-x} [12] measuring the ac susceptibility for low applied magnetic fields showed a cusp at a temperature we will label T_{SG}, not a singularity as a ferromagnetic transition would exhibit. Instead, it is the *nonlinear* susceptibility χ_{nl} that is diverging [60],

$$m = \chi h - \chi_{nl} h^3 + \cdots \tag{1.5}$$

as a divergent second derivative of a function would appear in the basic function as a

cusp. This does suggest that a different type of ordering is at work, so we look at a new order parameter,

$$q_{EA} = \frac{1}{N}\sum_i \langle S_i \rangle^2 \tag{1.6}$$

which instead of measuring the number of spins that are aligned with each other, measures how many spins are "stuck" in some position. The associated susceptibility,

$$\chi_{SG} = \frac{1}{N}\sum_{\langle i,j \rangle} \langle S_i S_j \rangle^2 \tag{1.7}$$

is directly related to the nonlinear susceptibility [6],

$$\chi_{nl} = \frac{1}{T^3}(\chi_{SG} - \frac{2}{3}) \tag{1.8}$$

so it diverges as well at the critical temperature. This type of ordering is the origin of the "glass" portion of the name spin glass. Instead of a standard ferromagnetic ordering, one has a magnetically disordered state that is instead ordered through its inability to change to a different state. This situation is analogous to how SiO_2, common glass, solidifies– not as a crystal, but as an amorphous solid lacking long-range order. In fact, this transition, that of structural glasses, is not well understood and we will return to this topic in (1.4).

Qualitatively, the glass transition in general can be explained in terms of the free energy "landscape". If one were to somehow map the free energy of a glassy system onto a continuous function of one generalized state variable, the resulting 2D plot would be reminiscent of a cross-section of rough geographical terrain, with mountains and valleys scattered about (Fig.1.2). The lowest point would correspond to a ground

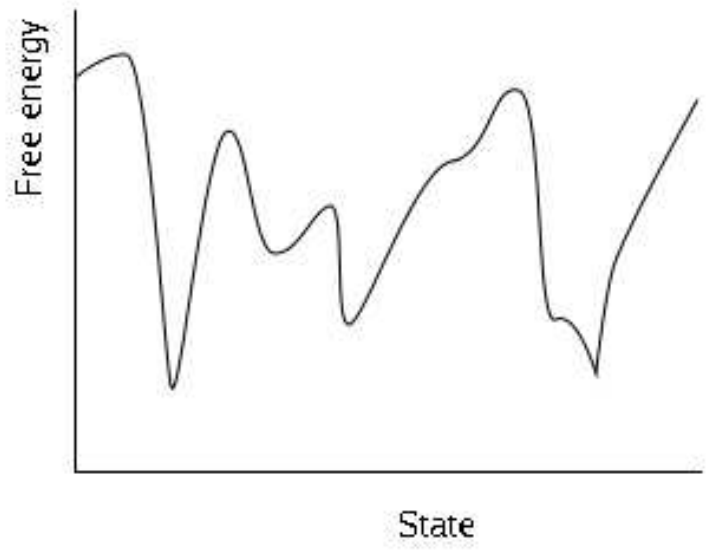

Figure 1.2: A qualitative picture of the free energy of a glass.

state (an ordered one in the case of structral glasses). There would also be other local minima, perhaps with only slightly greater free energy, but separated from the ground state by large barriers. In this picture, temperature corresponds to the height of the random jumps the system makes, so with sufficient heat these barriers can be crossed and the entire landscape can be traversed quickly. By reducing the temperature, one can severely hamper the ability of the system to explore distant states and the primary motion becomes restricted to the local basins.

1.3 Spin Glass Theory

Developing exact theoretical descriptions of spin glasses has proven to be a demanding task. Simply moving from the Ising ferromagnet to the EA glass has necessitated several new techniques. One of the primary goals is a theory that can be used to explain *real* spin glasses *i.e.* those in three dimensions on which one would be able to perform laboratory experiments. Presently, analytic solutions have been found only for models in one dimension (1D) and infinite dimensions. Through perturbative expansions and other approximations, theorists attempt to stretch these solutions to describe intermediate dimensions. Chapter 4 of this thesis will examine specific, competing predictions made by two leading theories.

The 1D EA glass can be solved with the renormalization group, pioneered by Wilson and Hogut. The nature of this technique is fairly straightforward to explain. Beginning with the Hamiltonian for the EA glass in a site-dependent field,

$$\mathcal{H} = -\sum_{\langle i,j \rangle} J_{ij} S_i S_j - \sum_i h_i S_i \tag{1.9}$$

one relates systems of different sizes to each other. For one dimension, a system of N spins can be exactly mapped to one with $N/2$ spins. The interactions and fields change: $J \rightarrow J'$ and $h \rightarrow h'$. By examing this *flow* of parameters, one can solve for fixed points, where the parameters do not vary with size. Any non-trivial ($0 < T < \infty$) fixed points correspond to a phase transition. An approximation technique from Migdal and Kadanoff (MK) [56, 36] applies these ideas at higher dimensions. For some specially constructed models, called hierarchical lattices, the MK method is exact, but for most

situations the method involves approximations which must be carefully analyzed. As the dimensionality increases, the approximations become more severe.

Based on renormalization group arguments for higher dimensions, a scaling theory was proposed and developed [2, 4, 55, 10, 11], which was also formulated in a different, equivalent manner by Fisher and Huse [17, 18, 31]. The approach of Fisher and Huse, which has been termed the "Droplet Picture"(DP), is phenomenological and considers the low-energy excitations above the ground state. These are termed *droplets* and are defined as minimal-energy clusters of size L. In zero field, the energy of such excitations are expected to scale as L^θ with θ the scaling exponent. This implies that spin-glasses models with a non-positive scaling exponent will not have a transition at non-zero temperature as large scale excitations above the ground state contribute negligible energy, thus destroying any order. For a non-disordered system like the ferromagnet, $\theta = d-1$ in dimension d since the minimal-energy excitations will be spherical. As expected, $T_c > 0$ only for $d \geq 2$ where $\theta > 0$. The DP prediction of $\theta \leq (d-1)/2$ for spin glasses indicates that the excitations have *fractal* surfaces. Unlike the ferromagnet, the minimal-energy surface for a droplet excitation in a spin glass is influenced by the disorder in the bonds, resulting in fractal geometry. Numerical results for θ for 2D give $\theta \simeq -0.28$ and for 3D $\theta \simeq 0.24$ [7], consistent with the lack of a 2D transition and the presence of one in 3D.

Other predictions of the DP include a characterization of the ground state structure and the existence of transitions in a field. It is suggested that in the DP the ground state is trivial. This can be illustrated with the *overlap distribution function*

$P(q)$ which gives the weight for each order parameter, *i.e.* a normalized measure of how many states have a given value of q (at a specific temperature). The DP ground state has

$$P(q) = \frac{1}{2}\delta(q - q_{EA}) + \frac{1}{2}\delta(q + q_{EA}) \tag{1.10}$$

where the only weight occurs at $|q| = q_{EA}$. When adding an external magnetic field, there is an extra contribution to the droplet energy. The zero-field magnetization of a droplet is a sum of L^d random numbers with value ± 1 with equal probability so the expected magnitude is $L^{d/2}$. Thus, applying a small field to the system will reduce the energy of half of the droplets by $hL^{d/2}$. Comparing this term to the surface energy defines a length scale

$$L \propto h^{-2/(d-2\theta)} \tag{1.11}$$

above which droplet excitations are energetically favored. As a result, any transition at a finite, non-zero T_c is destroyed. This prediction, the lack of a transition in a applied field, will be examined in Chapter 4.

Now we consider the *infinite*-dimensional version of the EA glass, where each spin interacts with every other spin. This is called the Sherrington-Kirkpatrick (SK) model [67] and is also theoretically tractable–this is due to the fully-connectedness of the spin network. The Hamiltonian is familiar,

$$\mathcal{H} = -\sum_{ij} J_{ij} S_i S_j \tag{1.12}$$

it differs from the EA glass only in its summation over *all* pairs i, j. Taken to the thermodynamic limit, $N \to \infty$, each spin has an infinite number of (nearest) neighbors.

It is in this sense that the SK model is like the EA model taken to infinite dimensions. When attempting to solve a ferromagnetic spin system, one common approximation is that of mean field theory (MFT). This approximation becomes exact when considering a system of infinite dimensions. Directly applying the same MFT methods to a spin glass does not make much sense, but the terminology is used to describe the exact solution to the infinite-dimensional case. Sherrington and Kirkpatrick provided such a solution to their model, however it was later shown to be unstable for the low-field, low-temperature portion of the H-T plane [14]. This region is bounded by the Almeida-Thouless (AT) line, as depicted in Fig(1.3). Later, this instability was resolved by a brilliant solution from Parisi [63] in his Replica Symmetry Breaking (RSB) model. In simple terms, RSB describes the ground state structure of a spin glass as an infinite collection of states that are not related by any obvious symmetry. Contrast this with the ferromagnetic Ising model (and the Droplet Picture) where symmetry is preserved and the ground state consists of just two choices related by a global spin flip. Specifically, the overlap distribution can be described as two delta functions at $\pm q_{EA}$ with a continuous interval of positive weight in between them see Fig.(1.4). The nature of $P(q)$ implies there are large-scale excitations between spin configurations whose energies remain finite as $L \to \infty$. From this it is assumed that these excitations involve domains with a *space-filling* surface.

Taken to be the correct solution of the SK model, there is an incentive to apply the RSB solution to lower dimensions, in the realm of real, physical systems. In order to test this applicability, one would look for the characteristics such as the AT line and

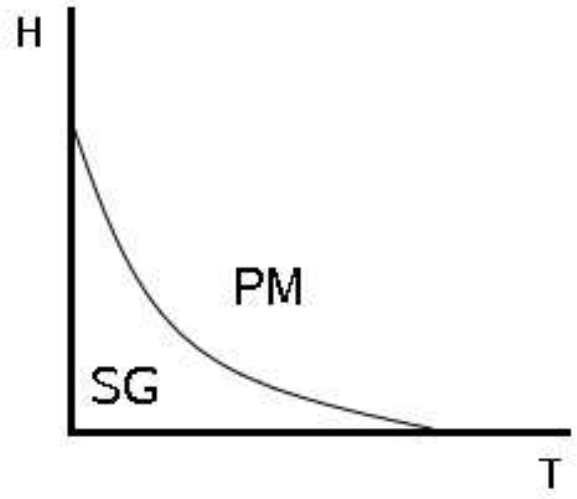

Figure 1.3: The AT line, separating the disordered paramagnetic (PM) region from a low-temperature, low-field spin-glass (SG) phase.

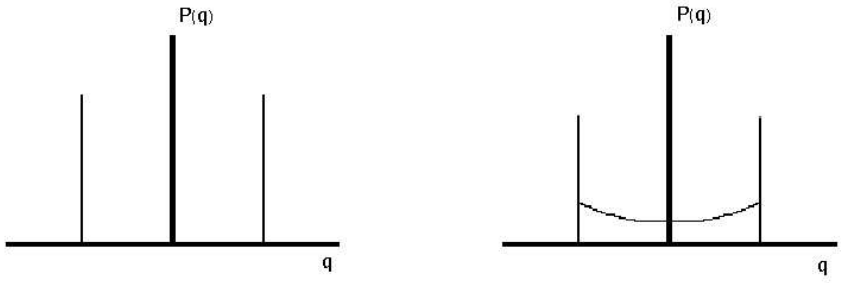

Figure 1.4: Pictorial representation of the ground state structure for the Droplet Picture (left) and Replica Symmetry Breaking (right).

the continuous portion of the order parameter distribution for low temperatures. We have performed investigations of this nature and the results are reported in Chapter 4.

1.4 Structural Glasses

Glass-forming liquids are those that undergo a kinetic arrest before they are able to rearrange into a crystalline state. This can be achieved in general by cooling a liquid sufficiently rapidly through the transition regime. Such scenarios are called *supercooling*. Standard window glass is a naturally-occuring example. The glass transition temperature T_G is, by convention, defined by the temperature at which a viscosity of 10^{13} Poise is reached. Below this temperature, laboratory experiments with glasses are dealing with essentially static systems. A range of behavior is observed in different glass formers undergoing cooling or a melt; if one brings different glasses above T_G, the rate of viscosity decrease can vary significantly and follow different functional forms. Such differences are due to the *fragility* of the glass. A strong (non-fragile) glass has a functional form for the viscosity that nearly obeys the *Arrhenius* law,

$$\eta = \eta_0 e^{B/T} \tag{1.13}$$

while fragile glasses are better described by a Vogel-Fulcher-Tamman form [72, 20, 69],

$$\eta = \eta_0 e^{B/(T-T_{VF})} \tag{1.14}$$

A qualitative picture of fragility is shown in Fig.(1.5).

There is a strong correlation between liquid's viscosity and the relaxation time– the decay constant τ in the autocorrelation function, which for high temperatures fits

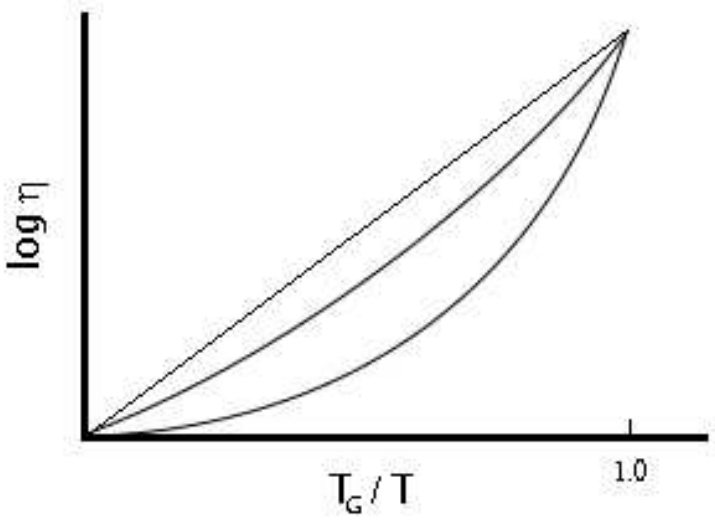

Figure 1.5: A qualitative look at glass fragility. Strong glasses are Arrenhian and show up as straight lines. Increased fragility causes increased curvature. Note the x-axis is given in inverse fractions of T_G so a melt would proceed right to left. All curves meet at $T/T_G = 1$ by definition.

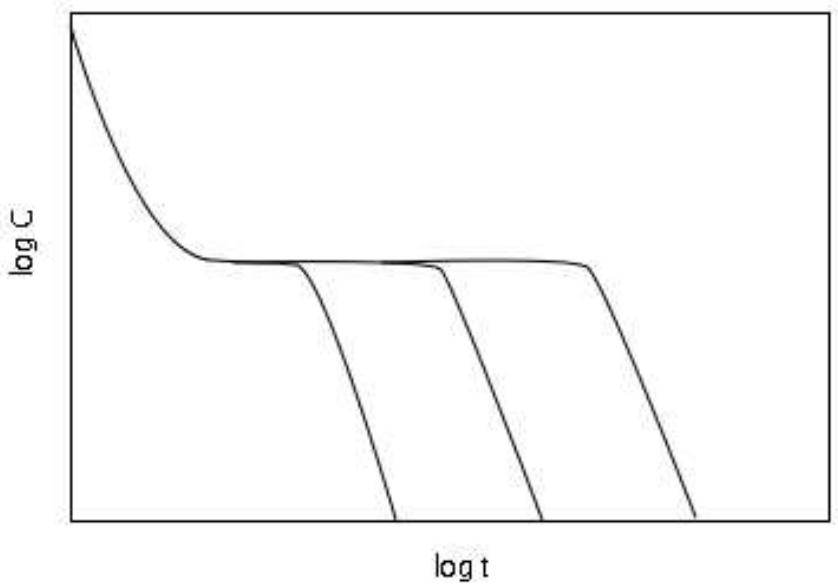

Figure 1.6: A sketch of glass behavior near T_G: relaxation in two modes α and β separated by a plateau. The β mode occurs prior to the plateau, the α afterwards. Different curves are shown to demonstrate the effect of increased waiting time, t_w, the rightmost curve having the largest t_w.

the form,

$$\langle C(t_w)C(t+t_w)\rangle \sim e^{-t/\tau} \tag{1.15}$$

This measures how similar a system is to a snapshot of itself a time t in the past. Note also the inclusion of t_w, the waiting time, which becomes important for systems that display *aging*. This is a feature of glasses and it highlights some interesting dynamics, the α- and β-relaxation modes (Fig.1.6). In terms of the energy landscape, the fast β modes correspond to motion within a local basin, while the slow α modes are the inter-basin moves–also called jump or activated processes.

By supercooling a liquid, an apparent *entropy crisis* appears. At the melting temperature T_M, the entropy of the liquid state is greater than that of the crystal by an amount ΔS_m (the entropy of fusion). Since the heat capacity of a liquid is greater than that of a crystal, with supercooling one can theoretically arrive at a temperature $T_K < T_M$, known as the Kauzmann temperature, where the entropy of the liquid state equals that of the crystal. Before further cooling, there clearly must be a change in behavior, as naive extrapolation to zero temperature would then suggest a negative entropy for the liquid. In practice, the glass transition $T_K < T_G < T_M$ halts the process. However, this scenario can be taken to suggest that an *ideal glass* forms at T_K, with an associated second-order phase transition. Further support for this hypothesis comes from a link to the dynamics: for most experimental systems, T_K is within ten percent of the value for T_{VF}, where the relaxation time hypothetically diverges.

Physicists today still lack a theory that provides a complete description of the features of structural glasses detailed above. Perhaps the most popular partial theory is the Mode Coupling Theory (MCT), which self-consistently arrives at equations of motion for the density fluctuation correlators [22, 5, 24]. It accurately captures dynamics above and near T_G. The original version of the theory predicted a complete kinetic arrest at a temperature T_D above T_G. This dynamical singularity is not found in real glasses, of course. Activated processes, allowing the system to jump between local energy minima, are still present. This is one failing of the so-called *idealized* MCT. Surprisingly, the MCT equations show up exactly as the dynamical mean field theory of some spin glass models involving *p-spin* interactions. In chapter 5, we discuss this

connection and investigate if the mean field behavior carries over to real dimensions.

The motivation behind exploring this analogy lies in the relative ease of spin glass simulation when compared to structural glasses. Spin glasses have much simpler state representations and the resulting dynamics are more easily adapted into numerical techniques. Simulating a structural glass requires working with interacting atoms, which ends up being rather cumbersome. Thus, if the physics are shared to a sufficient level, results for structural glass investigations can be more easily achieved by using spin glasses.

Chapter 2

Numerical Methods

With the advent of the computer, numerical calculations and simulations became the tools of choice for dealing with the harder problems in theoretical physics. Specifically, in the case of disordered systems, computer simulation is often by far the easiest and most direct way to learn about their behavior. This may be because theoretically the problem lacks an analytic solution and the approximations are of unknown accuracy; or experimentally, a certain observable is not accessible in the laboratory or a sample with the desired parameters cannot be manufactured easily. In these regards, computer simulation plays an important role filling the gaps where theory and experiment fail.

2.1 Monte Carlo

The expression for the equilibrium value of an observable Q is,

$$\langle Q \rangle = \frac{\sum_i Q_i e^{-\beta H_i}}{\sum_i e^{-\beta H_i}} \tag{2.1}$$

where each i represents a different state, and the sums are over all states. $\beta = \frac{1}{T}$ is the inverse temperature and H_i is the Hamiltonian, or energy, of state i. Often, one is interested in systems where the number of states is very large so that computing these sums is not feasible. Statistical sampling methods will approximate this by instead taking a smaller set of M measurements, where these M are drawn from the possible states according to a probability distribution p_i,

$$\langle Q \rangle_M = \frac{\sum_i^M Q_i p_i^{-1} e^{-\beta H_i}}{\sum_i^M p_i^{-1} e^{-\beta H_i}} \tag{2.2}$$

With a uniform sampling, one ends up with the a poor approximation as M will generally be much smaller than the number of states. Instead, if the measurements are made according to the following weight,

$$p_i = \frac{e^{-\beta H_i}}{\sum_i e^{-\beta H_i}} \tag{2.3}$$

the Gibbs-Boltzmann weight, we end up with a simple equation for the observable

$$\langle Q \rangle_M = \frac{1}{M} \sum_i^M Q \tag{2.4}$$

This is termed *importance sampling* and weights more heavily the terms with large contributions to the actual value. As a result, a more accurate approximation is

achieved. Simultaneously, the denominator in Eq.(2.3), known as the partition function, no longer has to be known. It should be noted that complete knowledge of the partition function allows one to calculate any equilibrium observables directly, thus there would be no longer any need for a simulation!

One way to generate states of a system with the states obeying a desired probablity distribution is to use a stochastic process that equilibrates to such a distribution. The Markov chain is a simple stochastic process where a new state is generated only from the knowledge of the current state. For example, a simple 2-state Markov chain can be represented by a 2x2 matrix containing the transition probabilities. For an Ising system with N spins, we have 2^N states and the corresponding transition matrix would have 2^N rows and columns each. By choosing appropriate transition probabilities, we can push a Markov chain to assume our desired equilibrium distribution of states.

A rule that achieves this is called *detailed balance*. For any two states, l and m, it says that the transition probability from $l \to m$, denoted by $w_{l\to m}$ follows

$$P_l^{eq} w_{l\to m} = P_m^{eq} w_{m\to l} \tag{2.5}$$

where P_l^{eq} is equilibrium probability distribution, generally set to be the Boltzmann distribution as produced by Eq.(2.3). This constraint admits a continuum of choices for the actual probabilities chosen, however detailed below are the two most common schemes.

The "Metropolis Algorithm" is perhaps the most used. It follows the formula

$$P(w_{l\to m}) = \begin{cases} e^{-\beta\Delta} & \Delta > 0 \\ 1 & \Delta \leq 0 \end{cases} \qquad \Delta = (E_m - E_l) \tag{2.6}$$

It is simple to see that it obeys detailed balance and is the choice that maximizes the transition probabilities for Ising spin systems. Another option is termed the "Heat Bath Algorithm" obeying

$$P(w_{l\to m}) = \frac{1}{e^{\beta\Delta}+1} \quad \Delta = (E_m - E_l) \tag{2.7}$$

which turns out to be a more efficient algorithm for some models, such as Potts systems with large p. There are some minor differences between the Metropolis and Heat Bath algorithms concerning their equilibration tendencies. In most finite temperature studies, however, the choice between the two methods doesn't seem to matter all that much; both produce reasonable results with comparable equilibration times. In the investigations presented here, we have defaulted to Heat Bath updating.

2.2 Parallel Tempering Monte Carlo

While importance sampling still forms the basis of most modern simulations, additional techniques have been developed to further improve the performance for difficult problems. Spin glasses are generally considered difficult because of the nature of their "energy landscape". The free energy of a spin glass, while in the spin glass phase, features many local minima separated by energy barriers of some characteristic magnitude. While simulating at low temperatures, the system has reduced ergodicity i.e. it

will only explore states around the local energy minimum. One is tempted to give the system a kick to allow it to escape. A development called "Replica Exchange" [30], now often referred to as Parallel Tempering (PT)–which will be the name used herein– is essentially a simple and efficient way of providing this kick without destroying detailed balance. It is based on the earlier method known as "Simulated Tempering" [23, 53].

In detail, the procedure involves M copies (replicas) of the system, each at a different temperature, simulated in parallel. The M temperatures are chosen such that the lowest T reaches some desired level, the highest T is such that $kT \gtrsim E_{barrier}$ ensuring that the system is able to explore its entire state space easily , and then the remaining T's cover the interior range. Standard spin updating techniques, such as those discussed above, are used in between a new type of update, the "global swap". This checks the replicas R_m at neighboring temperatures and swaps them in a Metropolis-like fashion

$$P(R_m \leftrightarrow R_{m+1}) = \begin{cases} e^{-\Delta} & \Delta > 0 \\ 1 & \Delta \leq 0 \end{cases} \qquad \Delta = (\beta_{m+1} - \beta_m)(E_m - E_{m+1}) \tag{2.8}$$

If working correctly, the replicas will travel in temperature space with a random-walk-type trajectory, each occasionally reaching the upper limit where they can freely move in state space. "Working correctly" implies that that *acceptance rates*–the probabilities that two neighboring replicas will swap–are sufficient. Ensuring that this is true for a given system requires some careful tweaking, and this topic will be explored in the context of optimization in chapter 3.

2.3 Equilibration

Using the methods detailed in the preceding section, we can converge upon equilibrium values for the desired observables. However, finding a reasonable time to *stop* the simulation is non-trivial. The most straightforward method is to measure an observable after different time intervals and wait until the data appear to have become stationary. In some cases where the measurements have large fluctuations, this may be hard to decide. Another method that is specific to systems with Gaussian interactions and fields, was developed [9, 39]. For a simple Hamiltonian

$$\mathcal{H} = -\sum_{\langle i,j \rangle} J_{ij} S_i S_j \tag{2.9}$$

where S_i denotes an Ising spin, J_{ij} a Gaussian interaction between two spins, and $\langle i, j \rangle$ summation over nearest neighbors. An expression for the average energy per spin is

$$U = -\frac{1}{N} \sum_{\langle i,j \rangle} [J_{ij} \langle S_i S_j \rangle_T]_{dis} \tag{2.10}$$

where N is the number of spins, $\langle \cdots \rangle_T$ indicates a thermal average (the type in Eq.(2.1)) and $[\cdots]_{dis}$ an average over the disorder, for example

$$[J_{ij}]_{dis} = A \int J_{ij} e^{-J_{ij}^2/2J^2} dJ_{ij} = 0 \tag{2.11}$$

with J the standard deviation of the J_{ij}. If we expand the disorder average in the equation for U, and choose to look at a single term U_{ij} it looks like

$$U_{ij} = -\frac{1}{N} \int J_{ij} \langle S_i S_j \rangle e^{-J_{ij}^2/2J^2} dJ_{ij} \tag{2.12}$$

where we can write the following

$$J_{ij}e^{-J_{ij}^2/2J^2} = J^2\frac{de^{-J_{ij}^2/2J^2}}{dJ_{ij}} \tag{2.13}$$

this differential can be shifted to the thermal average through integration by parts yielding

$$U_{ij} = -J^2\frac{d\langle S_iS_j\rangle}{dJ_{ij}} \tag{2.14}$$

Performing the derivative and summing over all U_{ij} gives

$$U = \frac{J^2\beta}{N}\sum_{\langle i,j\rangle}\left(1 - [\langle S_iS_j\rangle_T^2]_{dis}\right) \tag{2.15}$$

Thus by measuring the quantity

$$q_l = \frac{1}{N_{bonds}}\sum_{\langle i,j\rangle}[\langle S_iS_j\rangle_T^2] \tag{2.16}$$

which is termed the "link overlap", one arrives at a separate measurement of the energy.

$$U = -\frac{z}{2}\beta(1 - q_l) \tag{2.17}$$

with z representing the *coordination* (number of nearest neighbors) for a given spin in the lattice. Now, consider their behavior in a simulation. Assuming an initial state with uniformly random spins ($T = \infty$), the energy will be zero. The link overlap will also be zero, making the above expression $-\frac{z}{2}\beta$ which will be large and negative for low temperatures. As the simulation equilibrates, U will decrease as it approaches the correct $U(T)$ while the other form $U(q_l)$ will increase towards the same value and these quantities will eventually merge.

For models of the form,

$$\mathcal{H} = -\sum J_{ij} S_i S_j - \sum h_i S_i \tag{2.18}$$

where both J_{ij} and h_i are Gaussian-distributed, the method can be extended like

$$U = -\frac{z}{2}\beta(1 - q_l) - \beta(1 - q) \tag{2.19}$$

q being an observable called the "spin overlap" which is related to the EA order parameter,

$$q = \frac{1}{N}\sum_i [\langle S_i \rangle_T^2] \tag{2.20}$$

2.4 Overcoming Biasing in Monte Carlo

When using Monte Carlo to obtain measurements of an equilibrium value, the error takes the form

$$\langle Q \rangle_{MC} = \langle Q \rangle_{exact} + \delta_{MC} \tag{2.21}$$

with δ_{MC} being some random number with a random distribution symmetric about 0. A subsequent average over the disorder will tend to reduce this error as $N^{-1/2}$ for N samples. If we are interested in a squared quantity, then

$$\langle Q \rangle_{MC}^2 = \langle Q \rangle_{exact}^2 + 2\delta_{MC}\langle Q \rangle_{exact} + \delta_{MC}^2 \tag{2.22}$$

As the squared error term is non-negative, averaging over disorder will *not* reduce its magnitude. To circumvent this bias, one can measure the quantity Q with two independent simulations, and then take their product. For example, in the last section,

the link overlap, Eq(2.16) was introduced. An unbiased measurement would be

$$q_l = \frac{1}{N} \sum_{\langle i,j \rangle} S_i^\alpha S_j^\alpha S_i^\beta S_j^\beta \tag{2.23}$$

with "α" and "β" signifying different simulations. In general, an observable raised to a power k will require k different copies simulated. Most often this is done by introducing extra replicas at each temperature. For example, a PT simulation with M temperatures that measures a $\langle \cdots \rangle^4$ quantity will require $4M$ replicas in total.

2.5 Criticality and Finite Size Scaling

Much of the work within the study of spin glasses involves studying the critical behavior: determing the existence of phase transitions and estimating critical *exponents* which characterize the behavior near the transition. A major reason for this is the concept of *universality*: only a specific few input parameters to a model determine the critical behavior. For example, two spin systems with the same dimension and order parameter symmetry will share the same values of the critical exponents, assuming they both have a second order phase transition. Changing the other features, such as moving from a square lattice to a triangular one, won't affect this. Models sharing the same type of transition and the associated critical exponents form a *universality class*, and consequently fruitful analogies can be drawn between seemingly disparate models that both belong to the same class.

In numerical simulation, a method titled "finite size scaling"(FSS) is one of those preferred for extracting information on critical temperatures and exponents. We

begin with the critical behavior of the correlation length. Near the critical temperature T_c, it obeys a power law of the reduced temperature t,

$$\xi \sim |t|^{-\nu} \quad t = \frac{T - T_c}{T_c}. \tag{2.24}$$

For an infinite system this is fine, but the finite size of our simulations puts an upper bound on the correlation length that we actually measure (denoted with a subscript L) $\xi_L \leq L$. In a disordered phase characterised by short correlations, the ξ_L measured will generally represent the value as $L \to \infty$. When the system orders, long-range correlations form and ξ will saturate. This can be represented in the equation above with a *scaling* function, $g(x)$

$$\xi_L = Lg(\xi/L) \tag{2.25}$$

defined at the extremes of the function's domain to be

$$\begin{cases} g(x) = x & \text{x} \ll 1 \\ g(x) = const & \text{x} \gg 1 \end{cases}$$

which then contains the correct finite size behavior. Now we use our first equation to replace the ξ in the scaling function,

$$\xi_L = Lg(|t|^{-\nu} L^{-1}) \tag{2.26}$$

and then rescale the argument to g through a new function $\tilde{g}$,

$$\tilde{g}(x) = g(x^{-1/\nu}) \tag{2.27}$$

leaving

$$\xi_L = L\tilde{g}(L^{1/\nu} t) \tag{2.28}$$

where $\tilde{g}$ can now be extended to negative values of t. Based on this analysis, we should now calculate the quantity ξ_L/L, the dimensionless correlation length, for different system sizes and different temperatures. If the data agree across different L for a given temperature, then that temperature corresponds to $t = 0$ —in other words $T = T_c$. Once T_c is known, one can estimate ν by attempting to plot ξ vs $L^{1/\nu}t$. As the correct value of ν is approached the data will start to overlap, or *collapse*, to use common terminology.

The critical behavior of other observables can be expressed using similar arguments. For example, the susceptibility has a different critical exponent γ

$$\chi \sim |t|^{-\gamma}. \tag{2.29}$$

We can eliminate the dependence on t with the following,

$$\chi \sim \xi^{\gamma/\nu}. \tag{2.30}$$

From this we see that χ will itself reach a maximum value as ξ saturates. We can then borrow the scaling analysis from before and remove the dependence on ξ using something like Eq.(2.28),

$$\chi = \xi^{\gamma/\nu}\chi_0(L/\xi) \tag{2.31}$$

with the new scaling function defined as

$$\begin{cases} \chi_0(x) = x^{\gamma/\nu} & \text{x} \ll 1 \\ \chi_0(x) = const & \text{x} \gg 1 \end{cases}.$$

As ξ is not known beforehand, but L is, we modify the scaling function as follows,

$$\tilde{\chi}(x) = x^{-\gamma}\chi_0(x^{\nu})$$

which leaves us with

$$\chi = L^{\gamma/\nu}\tilde{\chi}(L^{1/\nu}t). \tag{2.32}$$

Assuming the critical temperature and ν have already been found, this equation then gives one a way to calculate γ.

Chapter 3

Optimization of Parallel Tempering

3.1 Motivation

In the previous chapter I introduced the method of Parallel Tempering (PT), which is a powerful tool for simulating systems with many local minima in the free energy. The method allows a system to travel in temperature, gaining the freedom to probe a larger region of configuration space by jumping between minima during its time at a high temperature. The temperatures used in a PT simulation are input by hand, which leads to the question of what specific temperatures to use. First, one clearly wants to contain the region of interest in the temperature interval, be it a transition temperature or simply the lowest value within one's computational budget. Second, as the prowess of PT relies upon crossing free energy barriers, the upper bound of the temperature interval should be placed in a region of rapid thermalization. Lastly, the acceptance ratio for swaps between neighboring temperatures should be *reasonable*–if

a low-temperature replica has a vanishingly small chance of reaching the upper bound, then the method is not being used to its full potential. Following these basic guidelines will be sufficient for some cases, especially with the rapid growth of available computing power. Still, there is a significant amount of freedom to choose among reasonable temperature sets, and for large-scale simulations–which can be on the order of months–it is worthwhile to consider optimizing this choice.

To begin optimization considerations, one must first identify the quantity to optimize. Within the parallel tempering scheme, a likely candidate is the round trip time–how many swaps a replica requires, on average, to reach both ends of the temperature interval. The round trip time will depend strongly on the acceptance rates, of which one must understand the physics. When simulating a system at a fixed temperature, the observed energy will fluctuate about some mean value. The magnitude of these fluctuations are related to the specific heat,

$$C = \frac{dE}{dT} = \frac{1}{T^2}\left(\langle E^2\rangle - \langle E\rangle^2\right) \tag{3.1}$$

$$\sigma_E = T\sqrt{C} \tag{3.2}$$

A swap move between two replicas at neighboring temperatures has an acceptance likelihood related to the amount of overlap in their fluctuations i.e. the amount of shared state space they explore (see Fig.(3.1)). The separation in energy between replicas at temperatures T_1 and T_2 will be

$$\Delta E = \int_{T_1}^{T_2} C(T)\, dT \tag{3.3}$$

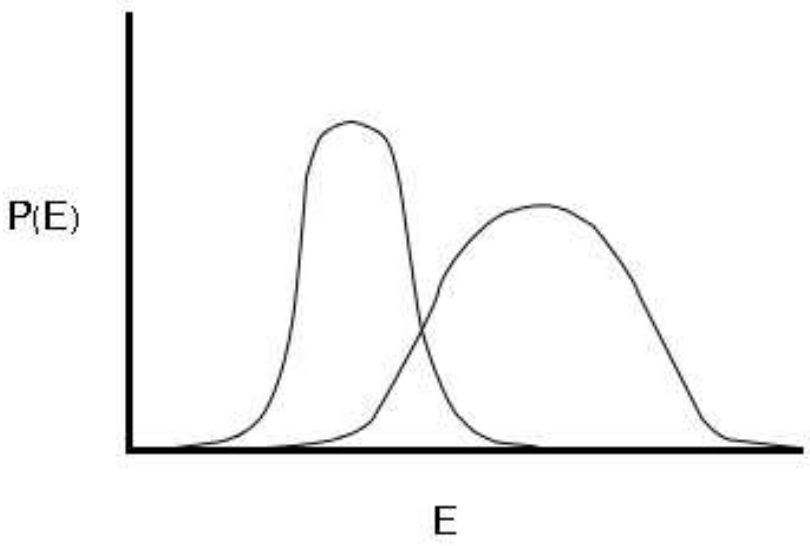

Figure 3.1: A sketch of two energy distributions at nearby temperatures. Swapping replicas between these temperatures will have average acceptance rates proportional to the amount of shared area.

Assuming a flat specific heat, the amount of overlap is proportional to,

$$\frac{\sigma_E}{\Delta T\, C} = \frac{T}{\Delta T\sqrt{C}} \tag{3.4}$$

which can be made clearer by using the intensive quantity $c = C/N$, the specific heat per spin,

$$p_{swap} = \frac{T}{\Delta T\sqrt{cN}} \tag{3.5}$$

and now the expected dependence on the number of spins N appears.

Then, assuming a constant acceptance rate across all intervals minimizes the round trip time, one might use a *geometric* temperature set, with spacings increasing as T increases. As the ultimate cost is based on CPU usage, the specific value chosen for the acceptance rate will reflect a compromise between reducing round trip time by interspersing more temperatures into the simulation and minimizing the CPU required by those extra replicas. One study suggested a hard value of 23% [46].

However, the calculation of acceptance probabilities is more complicated than this [66]. Also, the assumption that a flat acceptance rate minimizes round trip time fails to account for features in the specific heat. An adaptive algorithm that takes these problems into account is presented in Ref. [40]. This algorithm was applied succesfully to some simple systems, however it was not clear if it could be applied to spin glasses with any success. The following sections detail the investigations into this question.

3.2 Feedback Algorithm

First, we introduce some formalism to the analysis of round trips in PT replica space. Let the minimum and maximum of the temperature set used be denoted T_1 and T_M respectively, for a set of M temperatures. To track the motion of replicas, give them a label when they visit an extremum–any replica at T_1 gains the "up mover" label and any at T_M becomes a "down mover". An up(down) replica visiting $T_1(T_M)$ retains its label, and initially, replicas not at an extremum will be unlabelled. A histogram is kept of what label is occupying a given temperature–for example, after each global swap, the bin $n_{up}(T_i)$ is incremented if there is an up mover at T_i. From these histograms, define

$$f(i) = \frac{n_{up}(T_i)}{n_{up}(T_i) + n_{down}(T_i)} \tag{3.6}$$

which simply tracks the ratio of up movers at each temperature. By definition, $f(1) = 1$ and $f(M) = 0$ and it is a fair guess that in between there will be relatively smooth behavior. One can imagine that this quantity will say something about how well the replicas are circulating; if the ratio of up movers is very high at low temperatures but vanishes at high temperatures, e.g. f(i) being approximately a step function, the simulation is not proceeding efficiently. The temperature set could be optimized to bring more up movers to higher temperatures. We are interested in a theoretical f^{opt} that produces the fastest round trip times. For PT based on Metropolis updating, it is shown [70, 40] that the following

$$f^{opt}(i) = 1 - \frac{i-1}{M-1} \tag{3.7}$$

will maximize the replica current, which in turn may be expected to minimize round trip time. This expression is simply a linear decay in the up-moving fraction with increasing temperature index. To arrive at the temperature set that produces such behavior for a given system, a feedback algorithm was developed that, for a reasonable input set, will converge to the optimal one relatively quickly. The algorithm goes as follows:

- Initialize the histograms $n_{up}(T_i)$ and $n_{down}(T_i)$ to zero for all i
- Perform a PT simulation with N_{sw} global swap moves. After each, update the labels and histograms.
- Estimate a new temperature set based on the new $f(i)$
- Double the number of swaps $2N_{sw} \rightarrow N_{sw}$
- Repeat from the beginning until converged

In their paper, Katzgraber et al apply this technique to two 2D Ising models, a ferromagnet and a fully-frustrated model. Both cases experience noticeable decreases in the round trip time compared to a flat-acceptance temperature set. Furthermore, the fractional improvement gets better as the system size increases making its application potentially quite powerful. Thus, a natural progression would be to try the method on spin glasses, notorious for long equilibration times. The paper introduces the investigation, but doesn't give results of applying the algorithm. We present findings from applying this optimization to a simple spin glass model.

3.3 3D Edwards-Anderson spin glass

We introduced in (1.2) the Edwards-Anderson (EA) model, featuring only nearest neighbor (NN) interactions with some probability distribution, commonly bimodal or Gaussian with zero mean.

$$\mathcal{H} = -\sum_{\langle i,j \rangle} J_{ij} S_i S_j \tag{3.8}$$

The 3D case with Gaussian interactions features a transition with $T_c \simeq 0.95$ [54] and is the model with which we will test the optimization algorithm.

As a disordered system, simulating the EA glass involves running separate simulations for many realizations of the bonds–each realization referred to as a *sample*– and the averaging these results. The first roadblock occurs when considering the two ways to deal with this: optimize the temperature set for individual samples or for the entire collection at once. The former should take into account sample- to-sample fluctuations more precisely, however each optimization results in a unique temperature set, with only the minimum and maximum values fixed. The data for intermediate temperatures may be unusable because now one cannot perform averages over the disorder–there is a single sample available for each of the temperatures. However, it would be possible to overcome this with more advanced analysis, such as reweighting techniques [59]. As many studies of spin glass systems are interested in data for the entire temperature range simulated, we opted to optimize the *common* temperature set. Using the equilibration test mentioned in Section 2.3, we applied the algorithm to a small system, $L = 4$, and the results are shown in Fig.(3.2). Equilibration is reached when the values

for U and $U(q_l)$ agree. Instead of any reduction in the apparent equilibration time, there is a modest *increase*. We find similar behavior for $L = 6, 8$.

To understand this behavior, we look at the effect of the algorithm on the round trip times τ. Plotting the ratio τ_{opt}/τ_o versus τ_o in Fig.(3.3) for many samples provides a handle on the situation. The horizontal dashed line represents the break-even point, where the optimization had no effect on the round-trip time. First, note the distribution of the unoptimized times, which peaks around 700 (replica swaps) and has a modest tail to longer times. It is clear that there will be no overall improvement since the peak of the distribution mostly responds badly to the optimization. As one moves down the tail, the situation is even worse. This trend is more easily seen in Fig.(3.4) which bins the data along the x-axis and plots the median.

One variable not yet addressed is the number of sweeps to start the feedback cycle at i.e. the initial value of N_{sw}. This was studied, and it was simultaneously found that doubling the number of sweeps for each iteration cycle was generally an overkill, so Fig.(3.4) shows use of the algorithm with a *constant* number of sweeps per iteration. The findings suggest that the round trip times can be continually improved by spending large amounts of CPU time optimizing the temperature set. However, they remain worse than the unoptimized values for significant time spent in the optimization process, and the amount of time to equilibrate the 3D EA glass with the unoptimized temperature set is only $\mathcal{O}(10^4)$ for this size, making optimizations of this magnitude wasteful.

At this point it is still unclear *why* most samples are worsened by the optimization algorithm. However, by examining directly the random walks of individual,

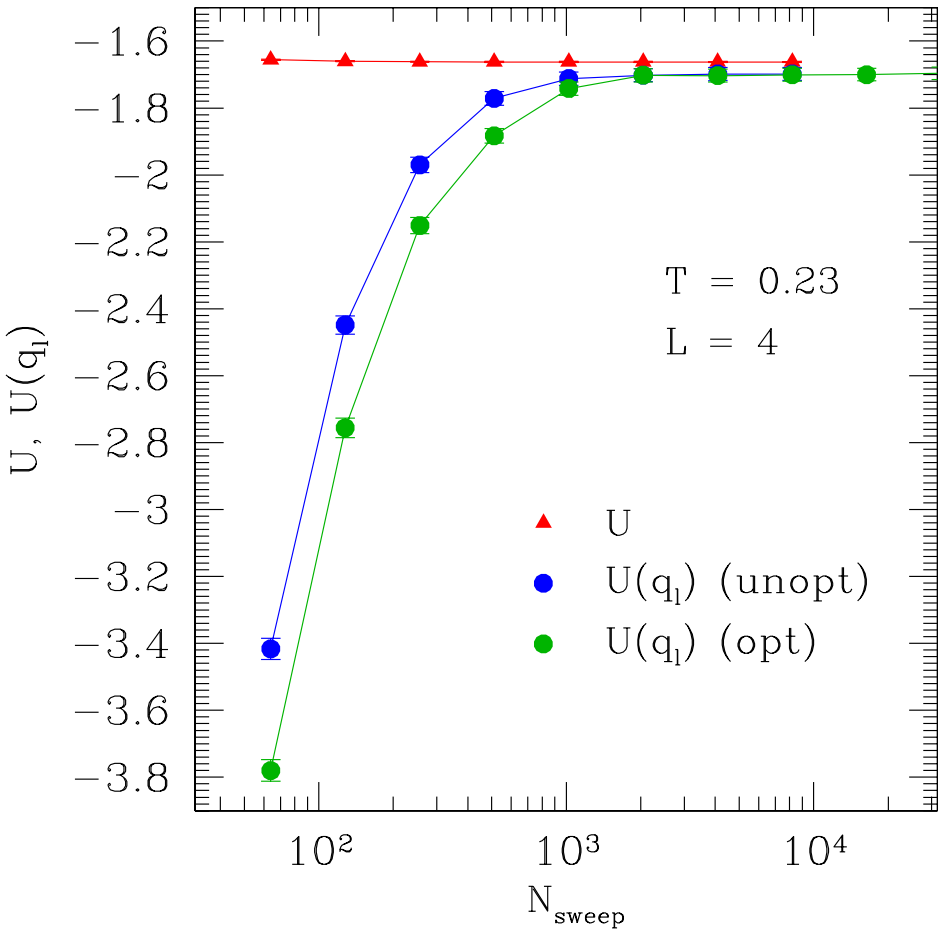

Figure 3.2: Comparison of equilibration of an EA glass, size L=4, using unoptimized and optimized temperature sets. Note that the optimized set produces *worse* equilibration.

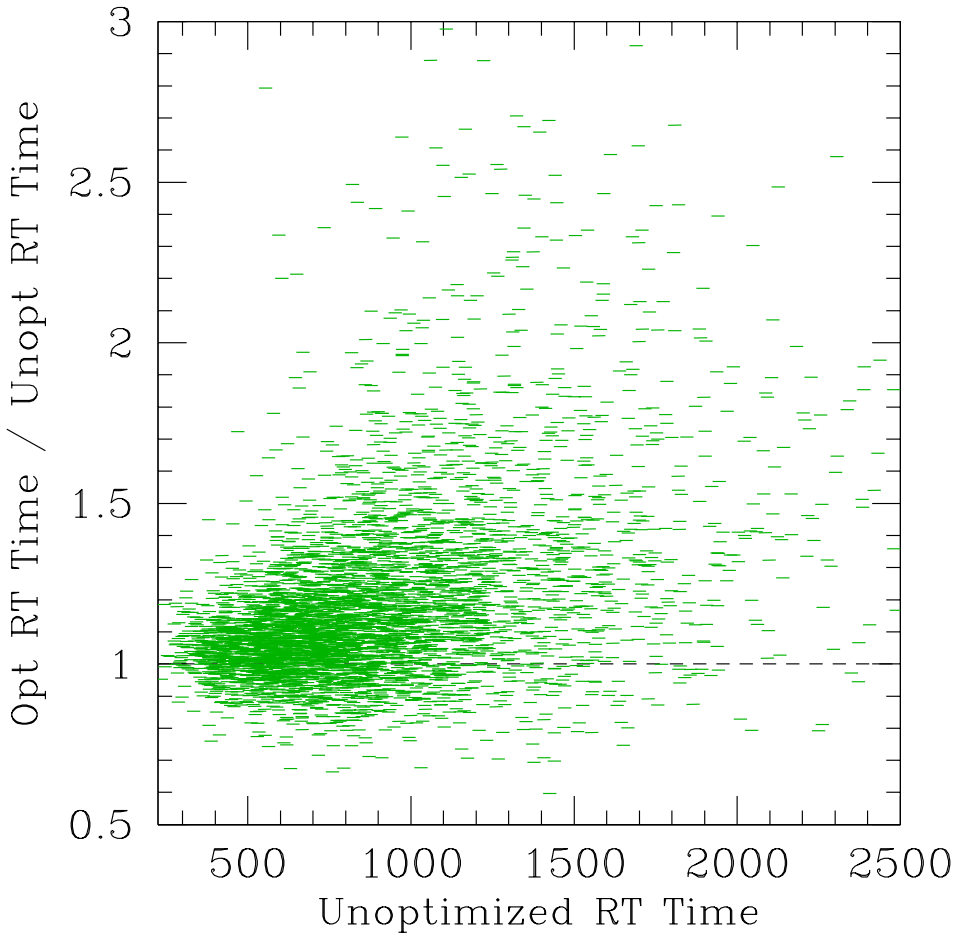

Figure 3.3: Scatter plot of RT time ratios for L=6. The dashed line indicates the break even point. Not only is the bulk centered above this line, there exists a strong tail of worsening optimization for the hardest samples

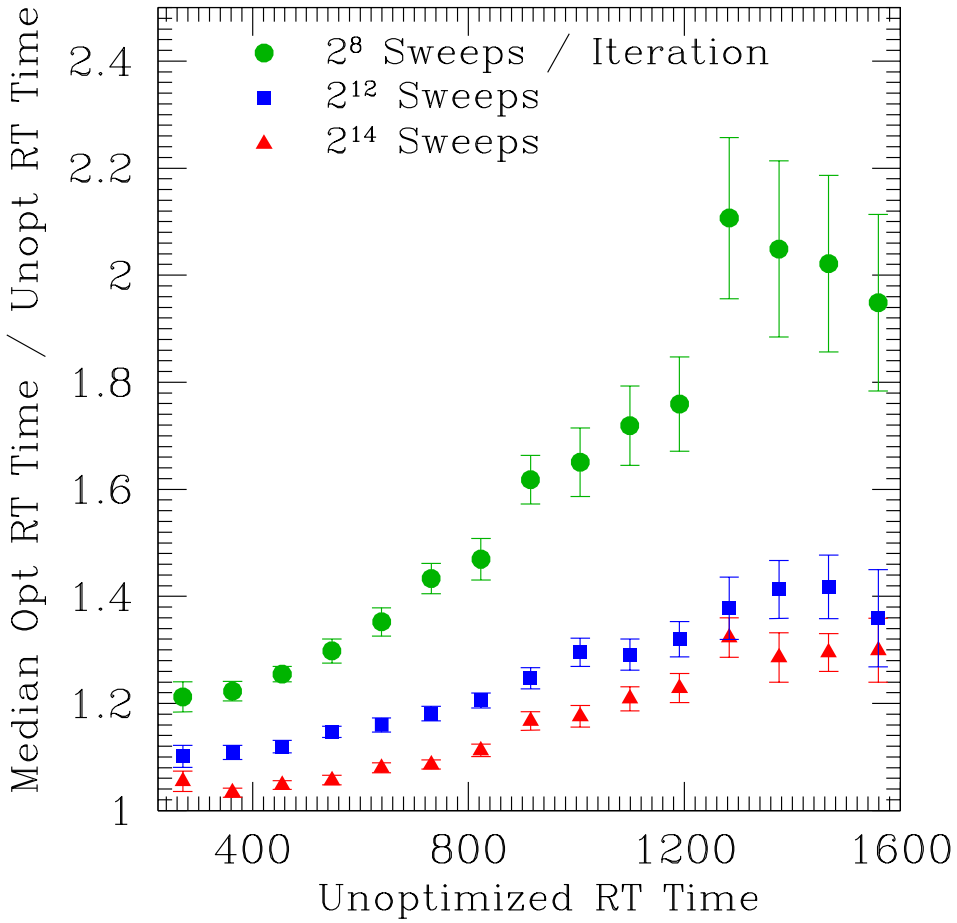

Figure 3.4: This plot is similar to Fig.(3.3) except the points are binned and instead the median is plotted. Note there are strong changes even between $N_{sw} = 2^{12}$ and $N_{sw} = 2^{14}$. These optimizations require CPU time on the order of the amount required to equilibrate this model unoptimized.

poorly optimized samples some idea of this can be gained. In Figs.(3.5) and (3.6) we see the change in walk behavior from optimizing the temperature set.

The first figure represents the unoptimized random walk of a sample that is known to optimize badly. A strong separation between two behaviors is clear. In one case, the replica remains in the upper temperatures, apparently unable to easily move below a certain point. The replica makes no round trips, since it never manages to reach the lowest temperature. However when inhabiting the lower region, it is able to occasionally travel to the highest temperature and return.

After optimization, there no longer exists separate regions of travel and replica current appears to be much larger. Yet, the replica has great difficulty reaching the temperature extremes, thus increasing the average round trip time. This example illustrates how the condition of increased replica current can be satisfied while not optimizing round trip time.

One major reason why this model and presumably most spin-glasses do not respond well to this optimization algorithm is the lack of any strong features in the specific heat, as seen in Fig.(3.7). The 2D Ising Ferrogmagnet has a divergent specific heat at its transition temperature, causing the widths of the energy distributions of each replica in temperature space to be very small. Then, when considering the optimal temperature set, the solution no longer follows from the naive assumption of a flat acceptance rate. However, since spin-glasses tend to have smooth specific heat curves, the simple approximation mostly holds.

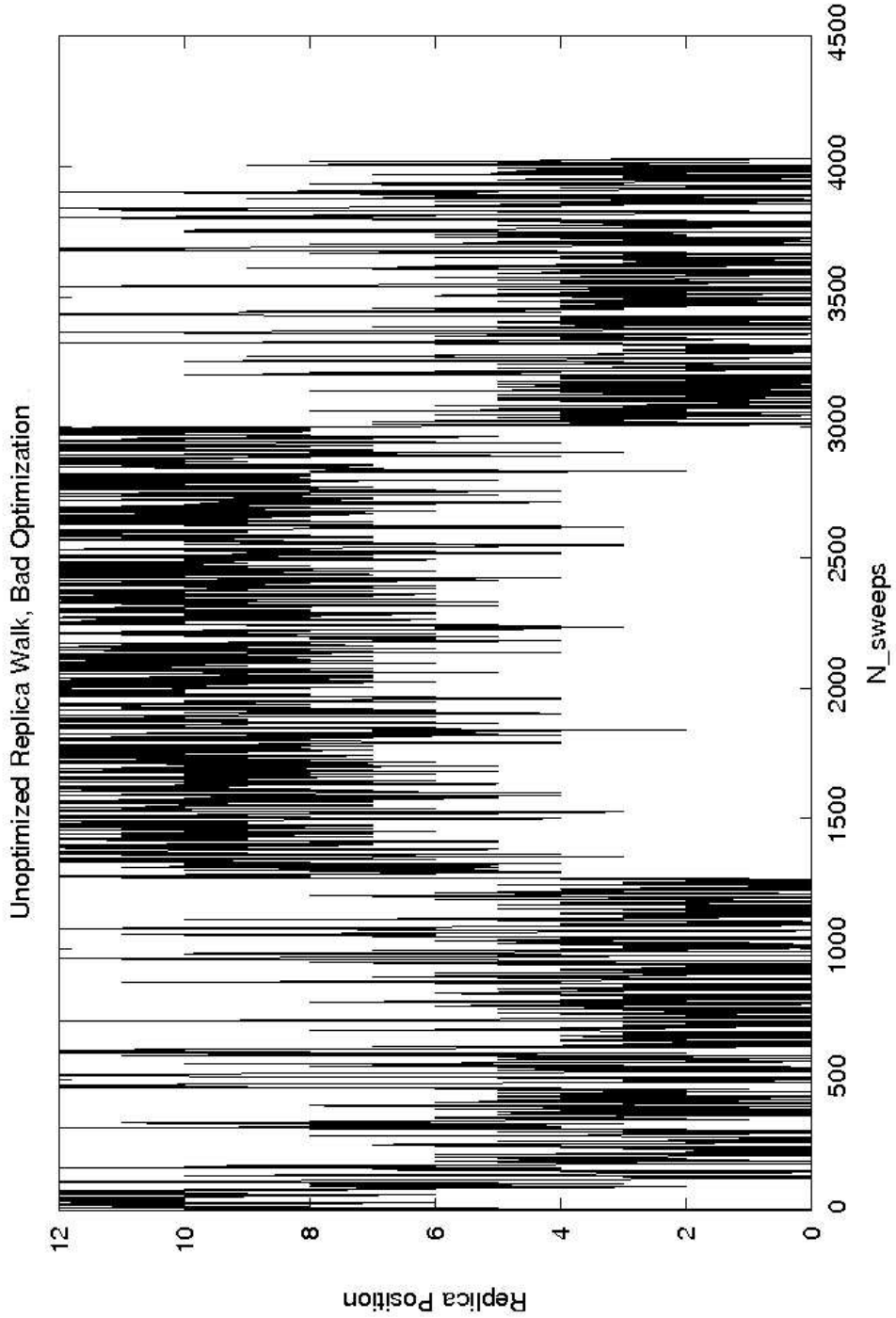

Figure 3.5: This shows the random walk of a replica from a sample that optimized poorly. The temperature extremes appear to be favored. Despite this, the replica is able to make a number of round trips.

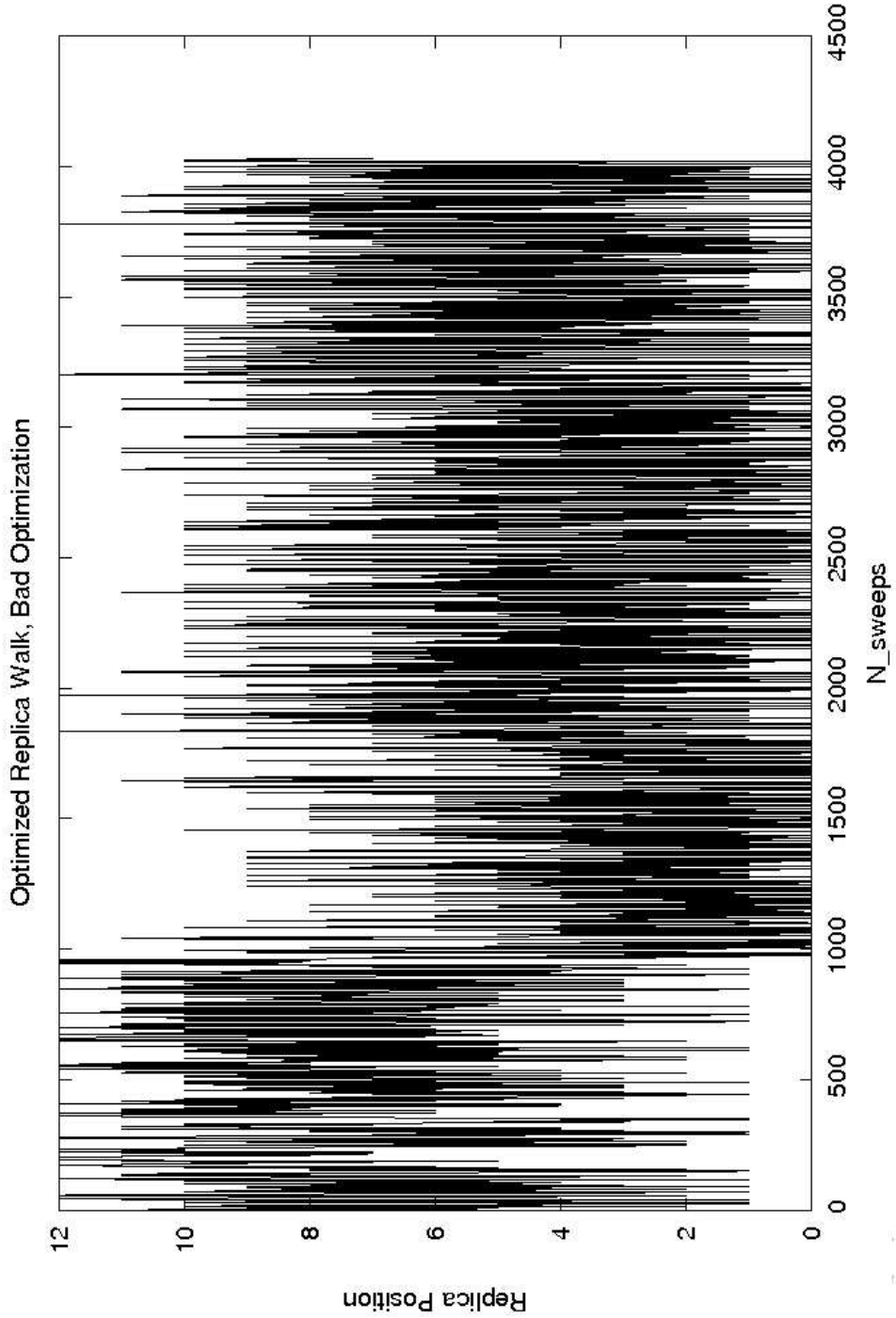

Figure 3.6: The same sample as in Fig(3.5), after optimization. The replica is now able to move more freely through the intermediate temperatures, apparently increasing the replica *current*, as the optimization method is designed to do. However, the number of round trips it makes is considerably reduced.

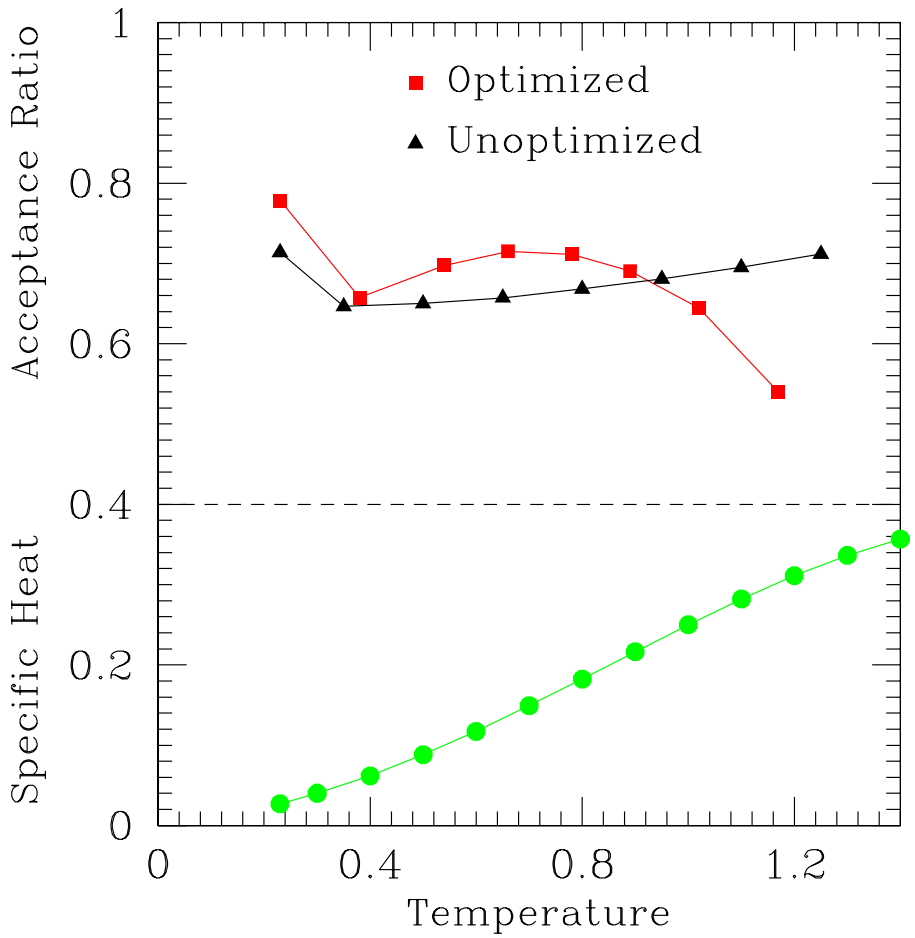

Figure 3.7: The top plots the acceptance rate for replica swaps before and after optimization. Increased rates for the middle temperatures after optimization fit with the qualitative change between Figs.3.5 and 3.6. The specific heat is plotted below, which is just to show it lacks any strong features.

3.4 Conclusion

Based on applying the feedback-optimized algorithm to the EA spin glass, we can say that the effectiveness of the proposed optimization technique will be diminished for spin glass models (relative to the models studied in Ref. [40]) for a number of reasons. First, the primary source of success for this algorithm in the test cases published in Ref.[[40]] is the divergent specific heat present in those models. Clearly, for for such systems, the optimization technique has shown to be powerful. Unfortunately, spin glasses tend to have smooth specific heat curves and cannot benefit in this regard. Second, the presence of disorder, and thus a need to simulate many different samples, motivates a consideration of only a *common* temperature set optimization, in many cases. This leaves strong sample-to-sample fluctuation in the round trip time mostly unaddressed. In turn, this causes slow convergence to the optimal temperature set, such that the amount of CPU time spent on the feedback algorithm rivals that of a standard, unoptimized simulation. Last, the present incarnation of the algorithm does not appear to address the edge effects properly, namely the replicas may have greater mobility but do not often reach the temperature extremes. Assuming a carefully chosen temperature interval, it will be important to use the entire range.

In conclusion, we find the applicability of the feedback-optimized algorithm to be minimal in the case of the EA glass, and likely spin glasses in general. Maximization of the replica current appears too weak of a condition; some other constraint is needed to reduce the final round trip times. If this can solved, then there may exist some cases

where it will be practical to use this technique.

Chapter 4

Study of the de Almeida-Thouless line using power-law diluted one-dimensional Ising spin glasses

4.1 Introduction

As discussed in Section 1.3, the MFT solution of the SK model suggests that an Ising spin glass has a line of transitions in an external magnetic field, the Almeida-Thouless (AT) [14] line. This instability line separates a high-temperature high-field paramagnetic phase where relaxation times—possibly very large—stay finite, from a low-temperature low-field phase where the energy landscape has valleys separated by truly infinite barriers in the thermodynamic limit. The applicability of concepts derived from the mean-field description of spin glasses to a variety of fields in science thus depends heavily on how well the mean-field picture reproduces the behavior of realistic

systems. This is particularly important when an external field is present because field terms are ubiquitous in nature.

Whether or not an AT line exists for real (short-range) spin glasses, is also a key feature distinguishing the two most popular scenarios for the nature of the spin-glass state below the (zero-field) transition temperature: the replica-symmetry breaking (RSB) picture of Parisi [64], and the "droplet picture" of Fisher and Huse [17, 19]. The RSB picture assumes that the behavior of real spin glasses is very similar to that of the mean-field solution [64] of the Sherrington-Kirkpatrick infinite-range model. Since the mean-field model has a stable spin-glass state in a field and thus has an AT line, it is proposed that this also occurs for more realistic short-range systems. By contrast, the droplet picture claims that large-scale excitations due to the applied field destroy any ordered phase above zero temperature. Specifically, a length scale is defined by the competition between the energies of the surface interactions of a droplet and the energy of its net magnetization. This length scale represents the droplet size above which field-induced fluctuations will occur, which section 1.3 discusses in detail.

Experimentally, it has been harder to determine if an AT line occurs than to show that there is a transition in zero field. For the latter case the divergence of the nonlinear susceptibility provides a clear signature of the transition, as discussed in section 1.3. Unfortunately, the nonlinear susceptibility does not diverge in a field, i.e., along the AT line. Instead, some studies have focused on the dynamical properties, by calculating the relaxation time through measurements of the AC and field-cooled susceptibilities [34]. If the relaxation time fits a power law about a temperature T_C,

called *critical slowing down*, T_C is deemed to be the critical temperature of a phase transition. In the case of $Fe_{0.55}Mn_{0.45}TiO_3$, which behaves as an Ising spin glass, Ref.[34] finds no transition. For zero field, the existence of a transition changes the functional form of the dynamical correlations from a stretched exponential (in the paramagnetic phase) to a power law (in the glass phase). That the application of a bias field returns the form to a stretched exponential is taken as evidence for no transition. Instead, evidence for a *dynamical crossover* is found where the characteristic length probed by the AC susceptibility reaches the length scale predicted by the droplet picture.

However, as noted in [74] there is a closely-related static quantity which diverges on the AT line and which can be measured in simulations, albeit not in experiments. A finite-size scaling analysis of the two-point correlation length indicated the absence of an AT line for three-dimensional (3D) Ising spin glasses [74, 35]. Subsequently, the same idea was applied to a one-dimensional (1D) model in Ref. [41] (referred to from now on as KY), in which every spin interacts with every other spin in the system with a strength which falls off with a power of the distance. By varying the power, one can simulate the whole range of possible behaviors [49, 19, 41], from infinite-range, through mean field, to non-mean field and finally to the absence of a finite-temperature transition. This is analogous to changing the space dimension d of short-range finite-dimensional models. KY found that an AT line does occur in the mean-field case (for short-range systems that would be for $d \geq 6$), but not in the non-mean-field case ($d < 6$).

4.2 Model and Observables

The model studied by KY is fully connected, i.e., the CPU time for one Monte Carlo sweep (MCS) grows as $\mathcal{O}(L^2)$, where L is the number of spins. This is inefficient for large L. Recently, this difficulty was removed in an elegant way in Ref. [50] by diluting the interactions and fixing the connectivity z. We thus study:

$$\mathcal{H} = -\sum_{i,j} \varepsilon_{ij} J_{ij} S_i S_j - \sum_i h_i S_i \ , \tag{4.1}$$

where $S_i = \pm 1$ are Ising spins evenly distributed on a ring of length L in order to ensure periodic boundary conditions. The sum is over all spins on the chain and the couplings J_{ij} are randomly distributed with zero mean and standard deviation unity (independent of distance). We take a Gaussian distribution. The dilution matrix ε_{ij} takes values 1 or 0, and a nonzero entry appears with probability p_{ij}, where $p_{ij} \sim r_{ij}^{-2\sigma}$ with $r_{ij} = (L/\pi)\sin(\pi|i-j|/L)$ representing the geometric distance between the spins. The power σ is a key parameter of the model. To avoid the probability of placing a bond being larger than 1, a short-distance cutoff is applied and thus we take

$$p_{ij} = 1 - \exp(A/r_{ij}^{2\sigma}) \ , \qquad z = \sum_{i=1}^{L-1} p_{iL}. \tag{4.2}$$

The constant A is determined numerically by fixing the average coordination number $z_{\rm av}$, set to six in this study. Note that this model has the same long range interactions on average, $[J_{ij}^2]_{\rm av} \sim 1/r_{ij}^{2\sigma}$, as in KY, but has only $Lz/2$ bonds rather than $L(L-1)/2$. Hence the CPU time for one MCS scales as $\mathcal{O}(L)$ rather than $\mathcal{O}(L^2)$. This has allowed to us to study significantly larger sizes than in the previous study, increasing the largest

studied to L=2048 over L=512. It should be noted that for low temperatures, the gain in efficiency from using the diluted model can be offset by the need to simulate lower temperatures. In order to compare temperatures simulated by the two models, we can scale the temperatures from the diluted model by $\frac{1}{\sqrt{z}} \sim 0.4$, which is analogous to the scaling already performed in KY. It is often found that the rescaled T_C for the diluted model is slightly lower than that of the fully-connected model. Then, for especially low T_C values, this difference will lead to a noticeable increase in the equilibration time required for temperatures near the transition.

As in the fully-connected case [41], by varying σ one can tune the model in Eq. (4.1) from the infinite-range to the short-range universality class. For $0 < \sigma \leq 1/2$ the model is infinite-range in the sense that $\sum_j [J_{ij}^2]_{\rm av}$ diverges, and for $\sigma = 0$ it corresponds to the Viana-Bray model [71]. For $1/2 < \sigma \leq 2/3$ the model describes a mean-field long-range spin glass, corresponding—in the analogy with short-range systems—to a short-range model in dimension above the upper critical dimension $d \geq d_{\rm u} = 6$ [37]. For $2/3 < \sigma \leq 1$ the model has non-mean-field critical behavior with a finite transition temperature T_c. For $\sigma \geq 1$, the transition temperature is zero. We are interested in models which are not infinite-range, and which have a finite T_c, i.e. $1/2 < \sigma \leq 1$.

A rough correspondence between a value of σ in the long-range 1D model and the value of a space dimension d in a short-range model can be obtained from

$$d = \frac{2 - \eta(d)}{2\sigma - 1} \tag{4.3}$$

where $\eta(d)$ is the critical exponent η for the short-range model, which is zero in the mean-

field regime. Equation (4.3) has the following required properties (i) $d \to \infty$ corresponds to $\sigma \to 1/2$, (ii) the upper critical dimension $d_{\rm u} = 6$ corresponds to $\sigma_{\rm u} = 2/3$, and (iii) the lower critical dimension, which is where $d_l - 2 + \eta(d_l) = 0$, corresponds to $\sigma_l = 1$. For example, in 3D $\eta = -0.384(9)$ [28] and thus the corresponding exponent is $\sigma \simeq 0.90$.

In this study we use site-dependent random fields h_i chosen from a Gaussian distribution with zero mean $[h_i]_{\rm av} = 0$ and standard deviation $[h_i^2]_{\rm av}^{1/2} = H_{\rm R}$. The choice of Gaussian fields has the advantage that we can perform a detailed test for equilibration as presented in section 2.3 and Refs.[39, 41].

To determine the existence of an AT line, we compute the two-point finite-size correlation length [62, 3, 74]. For this we start by determining the wave-vector-dependent spin-glass susceptibility given by

$$\chi_{\rm SG}(k) = \frac{1}{L} \sum_{i,j} \left[\Big(\langle S_i S_j \rangle_T - \langle S_i \rangle_T \langle S_j \rangle_T \Big)^2 \right]_{\rm av} e^{ik\,(i-j)}, \tag{4.4}$$

where $\langle \cdots \rangle_T$ denotes a thermal average and $[\cdots]_{\rm av}$ an average over the disorder. The correlation length is then given by [41]

$$\xi_L = \frac{1}{2\sin(k_{\rm m}/2)} \left[\frac{\chi_{\rm SG}(0)}{\chi_{\rm SG}(\mathbf{k}_{\rm m})} - 1 \right]^{1/(2\sigma-1)}, \tag{4.5}$$

where $k_{\rm m} = 2\pi/L$ is the smallest non-zero wave-vector compatible with the boundary conditions. According to finite-size scaling (FSS),

$$\begin{aligned} &\xi_L/L \sim \mathcal{X}[L^{1/\nu}(T - T_c)] \,, \qquad \sigma > 2/3 \\ &\xi_L/L^{\nu/3} \sim \mathcal{X}[L^{1/3}(T - T_c)] \,, \quad 1/2 < \sigma \leq 2/3, \end{aligned} \tag{4.6}$$

with $\nu = 1/(2\sigma - 1)$ in the mean-field regime [49]. The mean-field form of the FSS analy-

sis becomes necessary due to problems in the standard renormalization group treatment when reaching the upper critical dimension. In analogy to the discussion in Ref.[33], the existence of irrelevant observables that, while vanishing under renormalization, produce singularities that must be accounted for by modifying the FSS relations. Hence, if there is a transition at $T = T_c$, data for ξ_L/L ($\xi_L/L^{\nu/3}$ in the mean field region) for different system sizes L should cross at T_c.

We also present data for $\chi_{SG} \equiv \chi_{\rm SG}(0)$, which has the finite-size scaling form

$$\chi_{\rm SG} \sim L^{2-\eta}\mathcal{C}[L^{1/\nu}(T-T_c)]\ , \qquad \sigma > 2/3$$
$$\chi_{\rm SG} \sim L^{1/3}\mathcal{C}[L^{1/3}(T-T_c)]\ , \quad 1/2 < \sigma \leq 2/3. \tag{4.7}$$

Hence curves of $\chi_{\rm SG}/L^{2-\eta}$ ($\chi_{\rm SG}/L^{1/3}$ in the mean-field regime) should also intersect. This is particularly useful for long-range models since η is given by the naive expression $2-\eta = 2\sigma - 1$ *exactly*.

As discussed in KY, for the simulations to be in equilibrium with Gaussian fields and bonds, the following equality must hold:

$$U(\hat{q}_l, q) = -\frac{1}{T}\left[\frac{N_b}{L}\,(1-\hat{q}_l)\right]_{\rm av} - \frac{H_{\rm R}^2}{T}(1-q), \tag{4.8}$$

where $q = L^{-1}\sum_i[\langle S_i\rangle_T^2]_{\rm av}$ is the spin overlap, $\hat{q}_l = N_b^{-1}\sum_{i,j}\varepsilon_{ij}\langle S_iS_j\rangle_T^2$ is the link overlap of a given sample, and N_b is the number of nonzero bonds of the sample. To avoid bias, each distinct thermal average is evaluated in a separate copy (replica) of the system with the same disorder. Because we need to compute the "connected" correlation function in Eq. (4.4) we simulate *four* replicas for each temperature. To speed up equilibration we use the exchange Monte Carlo method [23, 30]. Simulations

are performed at zero field, as well as at $H_{\rm R} = 0.1$, a value considerably smaller than $T_c(H_{\rm R} = 0)$ for the values of σ studied. For details see Table 4.1.

4.3 Results

We start by showing in Fig. 4.1 data for ξ_L/L against T for $\sigma = 0.75$ in zero field, for several system sizes. The data intersect cleanly at $T_c \simeq 1.50$ indicating a transition at that point, see Eq. (4.6). The inset shows $\chi_{\rm SG}/L^{2-\eta}$ using the exact value $\eta = 1.5$. Note that the temperatures at which the susceptibility and correlation length data cross are quite close to each other. This is taken as evidence that corrections to scaling are small here. While the calculation of ξ_L depends on $\chi_{\rm SG}$, it also depends on $\chi_{\rm SG}(k)$, so one expects ξ_L and $\chi_{\rm SG}$ to have differing magnitudes to their FSS corrections. Since the results agree well, both magnitudes are taken to be small.

For comparison we also show data in the mean-field regime where an AT line is expected to occur [41]. For $\sigma = 0.60$ and $H_{\rm R} = 0.1$ there is a clear intersection, see Fig. 4.2. The temperature of the intersections is slightly different in the two cases, about 1.60 for $\xi_L/L^{5/3}$ and about 1.75 for $\chi_{\rm SG}/L^{1/3}$, suggesting finite-size effects possibly due to long negative tails in the spin overlap distribution (see Fig. 4.6). Furthermore, the next figure (4.3) shows our data for an increased field $H_{\rm R} = 0.2$. Here, there is disagreement between the two analyses. It appears increasing the field strength has heightened the discrepancy in their FSS corrections. Presently, it is unknown which gives the correct result.

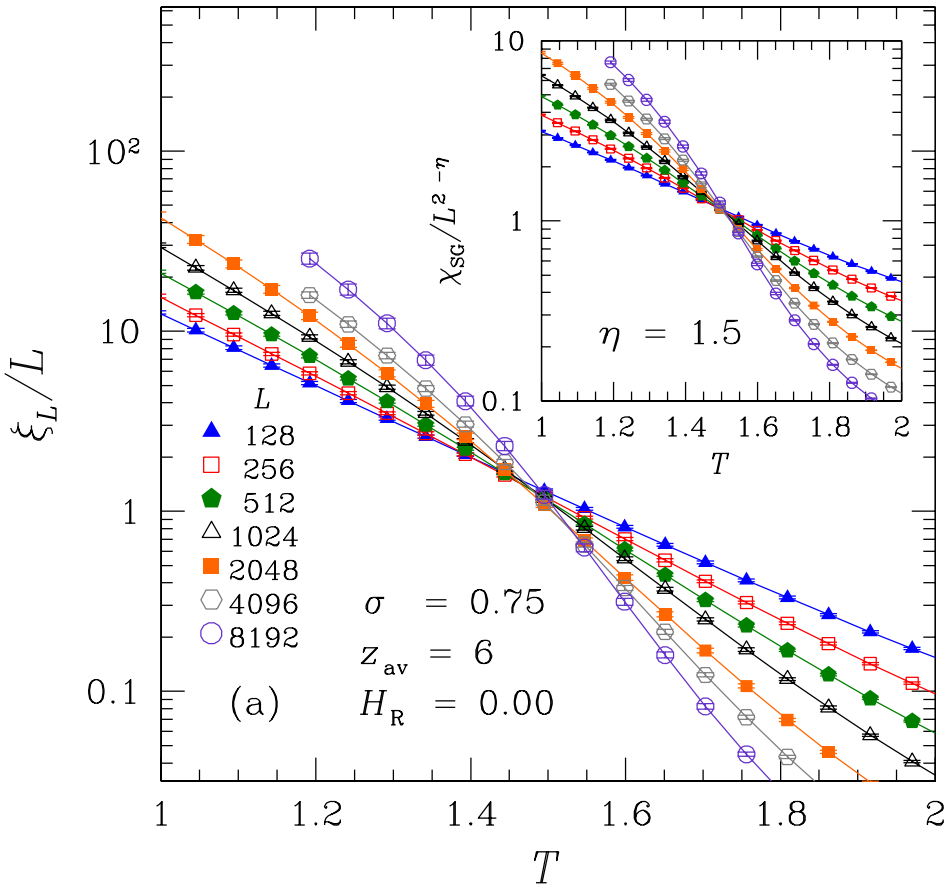

Figure 4.1: Finite-size correlation length divided by L as a function of T for different sizes for $H_{\rm R} = 0$ and $\sigma = 0.75$ (non-mean-field region). The inset shows $\chi_{\rm SG}/L^{2-\eta}$ using the exact value $\eta = 3 - 2\sigma = 1.5$. In both cases the data cross indicating a phase transition at zero field.

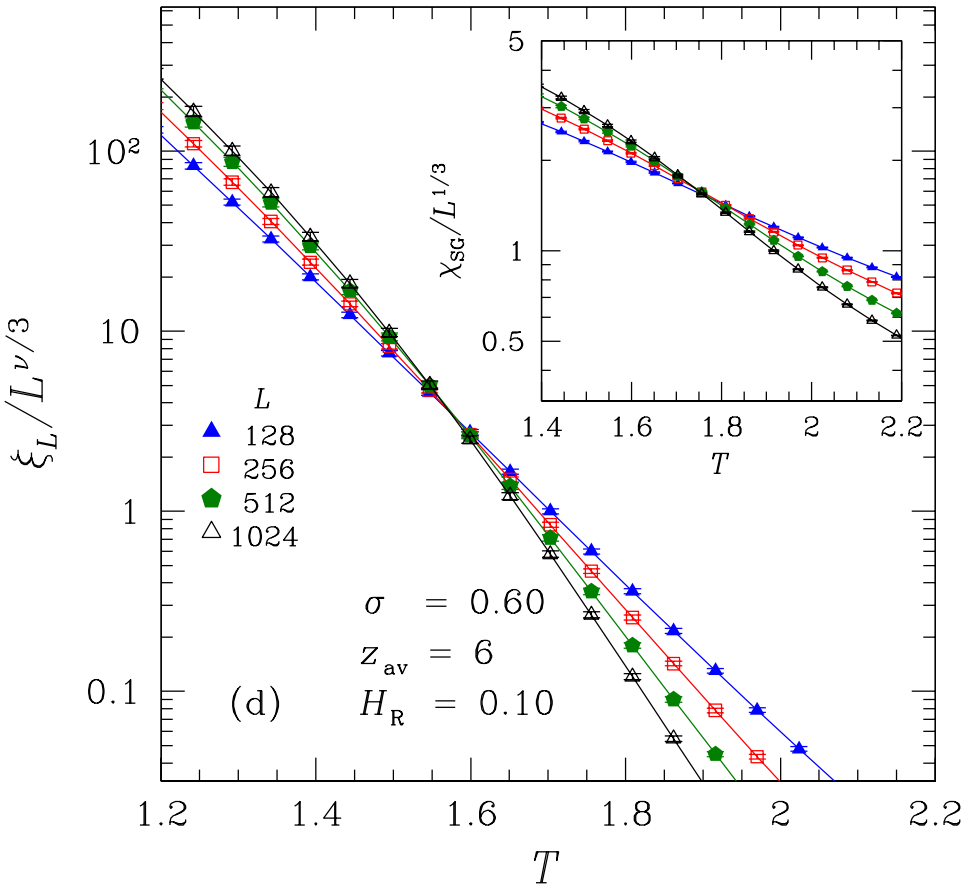

Figure 4.2: Data for the correlation length divided by $L^{\nu/3}$ ($= L^{5/3}$) as a function of T for different sizes for $H_{\rm R} = 0.1$ and $\sigma = 0.60$ (in the mean-field region). The inset shows $\chi_{\rm SG}/L^{1/3}$. The intersections show that there is a transition in a field, i.e., an AT line for this value of σ.

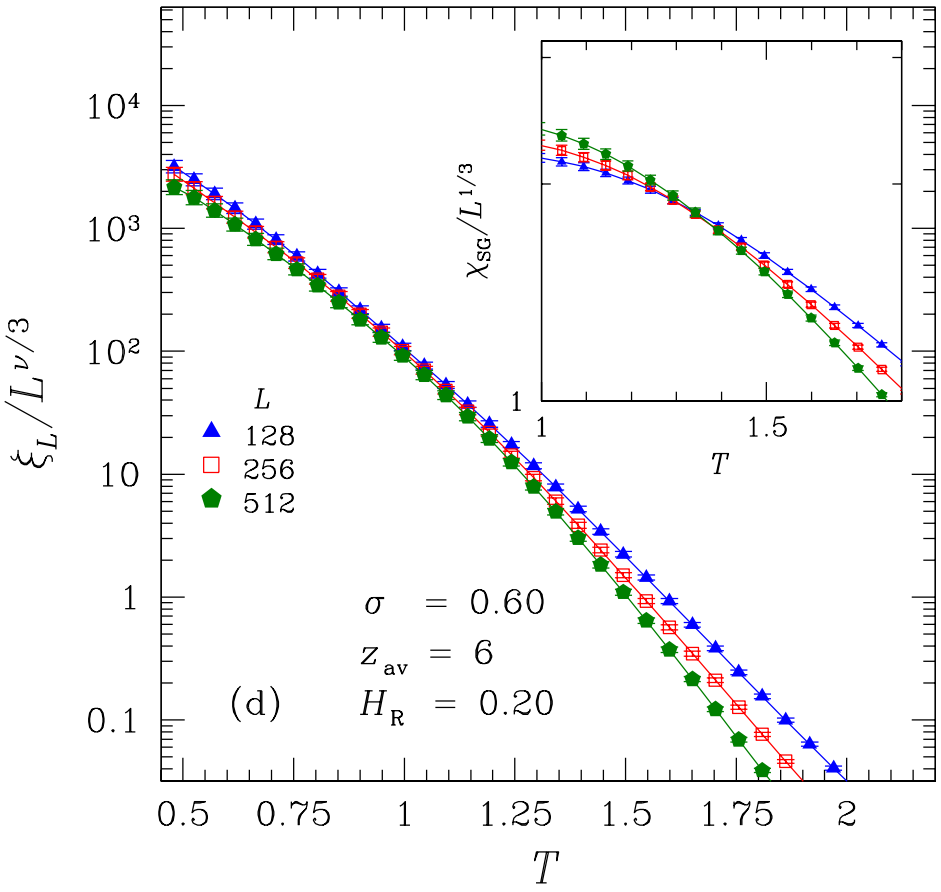

Figure 4.3: The same as (4.2) with the field increased to $H_{\rm R} = 0.2$. The xi_L/L and χ_{SG} analyses now give opposing results. It is not yet obvious which, if any, are accurate.

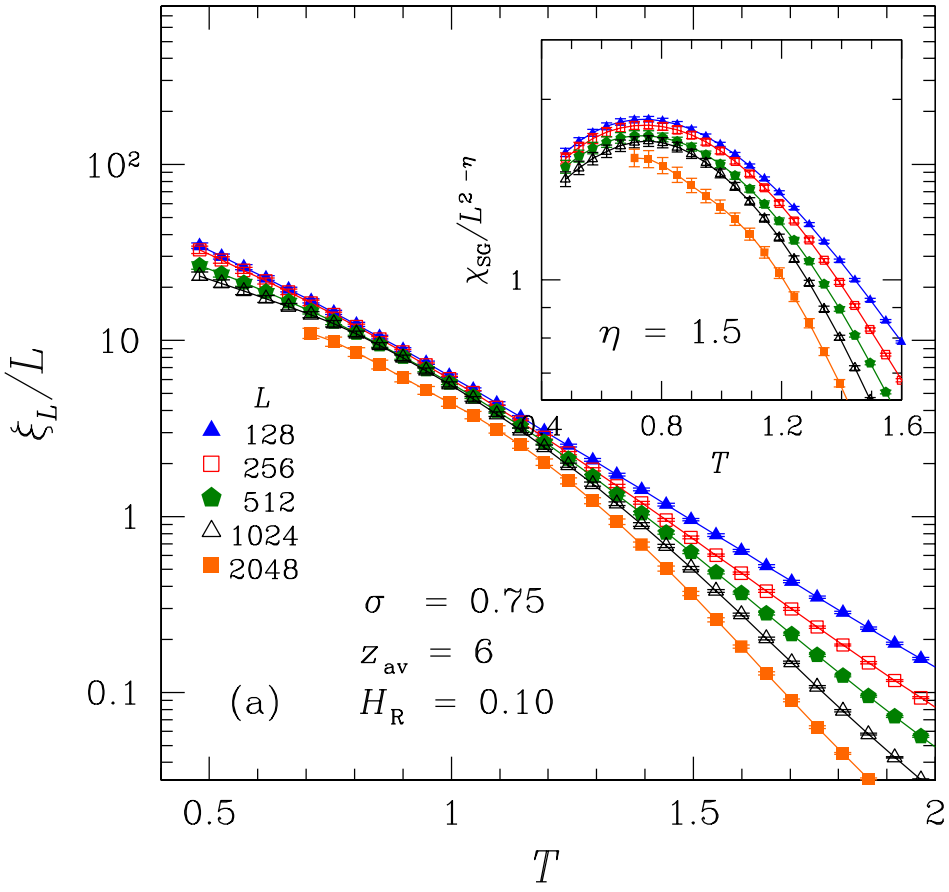

Figure 4.4: Same as (4.1) but for $H_{\rm R} = 0.1$. The absence of an intersection down to low T shows that there is no transition in a field [the shaded area corresponds to $T_c(H_{\rm R}) = 0$].

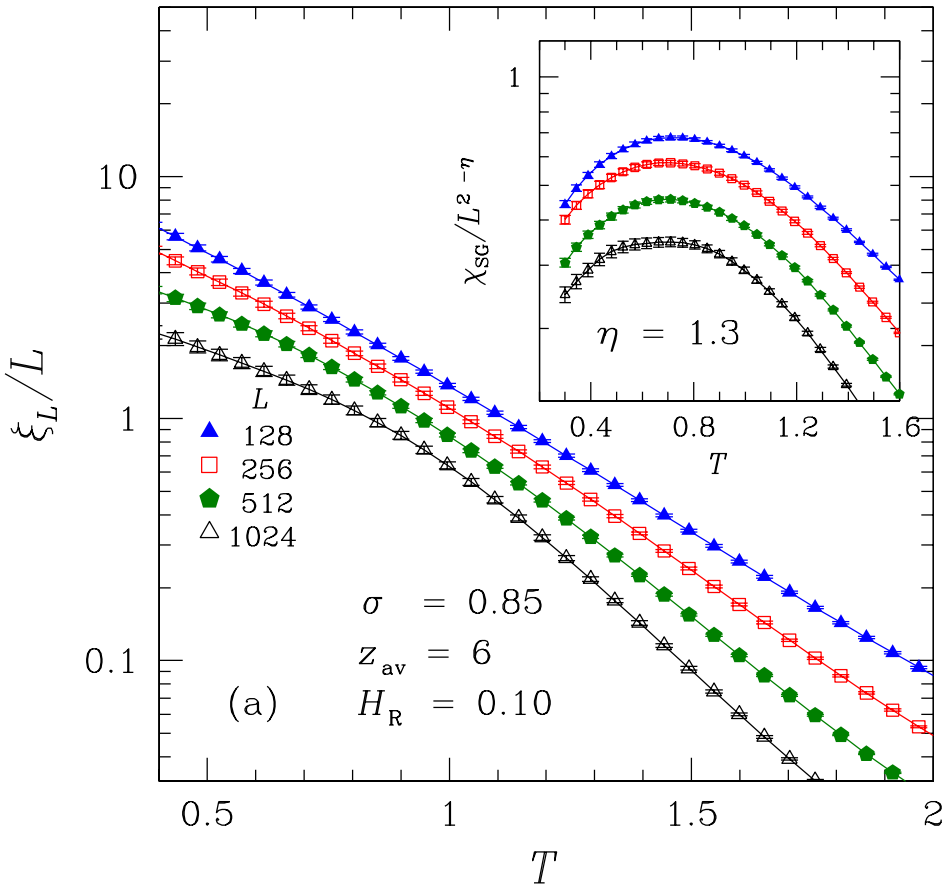

Figure 4.5: These data for $\sigma = 0.85$, i.e., deeper into the non-mean-field regime, clearly show the lack of a transition.

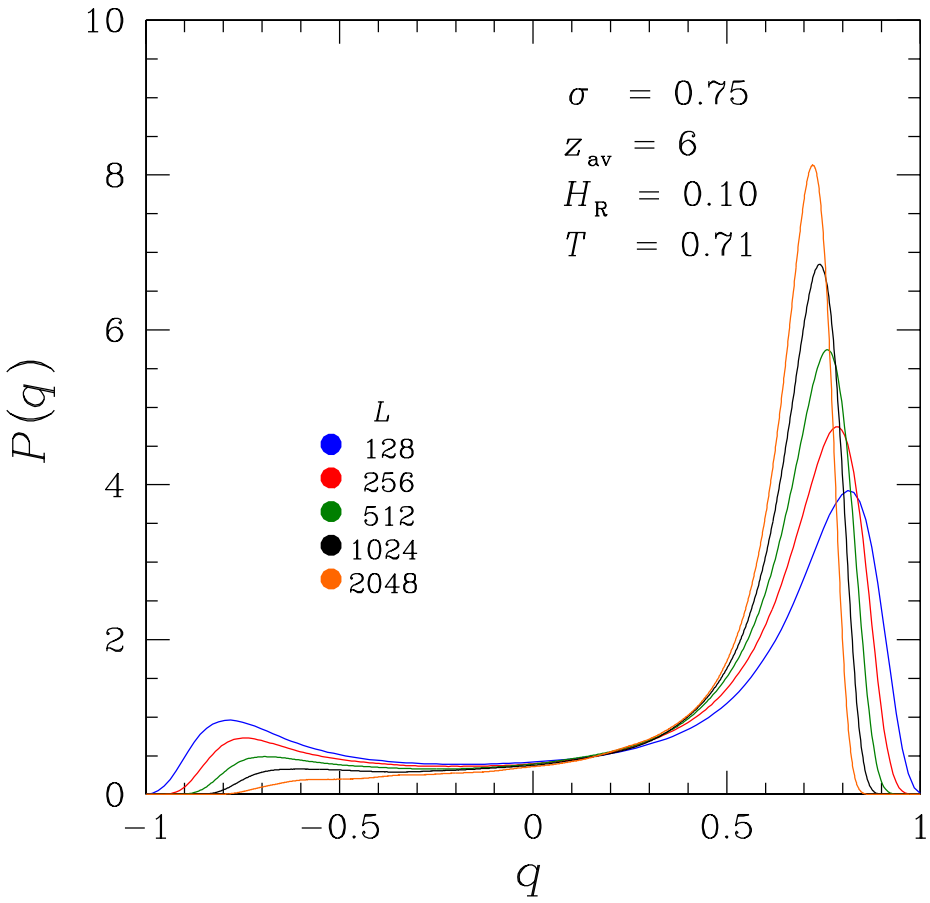

Figure 4.6: Distribution of the spin overlap q for $\sigma = 0.75$, $T = 0.71$ and $H_{\mathrm{R}} = 0.1$. Even for the larger L studied the negative tail extends into the negative region.

In contrast to Fig. 4.1, which shows the expected zero-field transition for $\sigma = 0.75$, Fig. 4.4 shows no intersections in a small field $H_{\mathrm{R}} = 0.1$ [approximately 0.067 of the zero-field T_c shown in Fig. 4.1]. Both analyses, ξ_L/L and χ_{SG}, agree in this case. This suggests there is no AT line for $\sigma = 0.75$, except possibly for even smaller values of the field.

We note that some other recent results from Leuzzi et al [51] come to different conclusions for a very similar model at the same value of σ. First, they calculate a correlation length from spin glass susceptibility data. This gives comparable results to ours. They claim these results are prone to strong finite-size corrections, showing a figure like Fig. 4.3. Then, they indirectly find χ_{SG} by measuring $\chi_{SG}(k)$ for many values of k and extrapolating $k \to 0$. The temperature where χ_{SG} diverges when taking $L \to \infty$ will be T_C. This analysis may be an answer to the large finite-size effects present in such data as Fig. 4.3. However, as it is a new technique, more supporting evidence is required to show its validity. Incidentally, in chapter 5 we study a model purported to be in the same universality class as the present one. Results for this model do find a transition for $\sigma = 0.75$ (see Fig. 5.2), using our same method involving ξ_L/L. Further discussion can be found there.

Note that $\sigma = 0.75$ is in the non-mean-field regime ($2/3 < \sigma < 1$). Whereas the data for $\sigma = 0.75$ for small sizes merge, and it is only for the larger sizes that the data do not even meet, for $\sigma = 0.85$—deeper in the non-mean-field regime—even the data for small sizes do not meet at any temperature down to $T = 0.30$, see Fig. 4.5. At this value of σ, one is reasonably close to three dimensional behavior, as studied in

Ref. [74] which agrees with these results. Also, the data from chapter 5 for this case agree qualitatively.

4.4 Summary

To conclude, we have studied the existence of an AT line using a long-range one-dimensional Ising spin-glass model. By simulating very large systems, we find that an AT line occurs in the mean-field region. It also seems well-supported that an AT line is absent from systems with a dimension near three, the region of primary interest. Of course, an AT line at extremely small fields cannot be ruled out. While this work and KY agree on the intermediate case $\sigma = 0.75$, there is enough uncertainty due to competing conclusions from similar investigations that we cannot make any strong claims. However, as the method used here is a familiar, proven technique—in contrast to Ref. [51]— with excellent statistics, substantial counter-evidence will be required to dismiss the results presented here.

Table 4.1: Parameters of the simulations for different field strengths $H_{\rm R}$ and exponents σ. $N_{\rm sa}$ is the number of samples, $N_{\rm sw}$ is the total number of Monte Carlo sweeps, $T_{\rm min}$ is the lowest temperature simulated, and N_T is the number of temperatures used in the parallel tempering method for each system size L. The last column shows the parameter A [Eq. (4.2)] fixing $z_{\rm av} = 6$ neighbors.

σ	$H_{\rm R}$	L	$N_{\rm sa}$	$N_{\rm sw}$	$T_{\rm min}$	N_T	A
0.60	0.10	128	8000	8192	0.480	46	0.99458
0.60	0.10	256	8000	32768	0.480	46	0.90363
0.60	0.10	512	5000	131072	0.480	46	0.83827
0.60	0.10	1024	5000	524288	0.480	46	0.78926
0.60	0.10	2048	4500	65536	1.393	26	0.75140
0.75	0.00	128	5000	32768	0.300	50	1.71141
0.75	0.00	256	5000	32768	0.300	50	1.64289
0.75	0.00	512	5000	524288	0.300	50	1.59859
0.75	0.00	1024	2900	2097152	0.300	50	1.56903
0.75	0.00	2048	1000	2097152	0.480	46	1.54892
0.75	0.00	4096	1000	65536	1.192	31	1.53506
0.75	0.00	8192	500	131072	1.192	31	1.52544
0.75	0.10	128	5000	32768	0.480	46	1.71141
0.75	0.10	256	5000	131072	0.480	46	1.64289
0.75	0.10	512	5000	262144	0.480	46	1.59859
0.75	0.10	1024	5000	524288	0.480	46	1.56903
0.75	0.10	2048	2800	524288	0.710	39	1.54892
0.85	0.10	128	6000	16384	0.300	50	2.39485
0.85	0.10	256	6000	65536	0.300	50	2.34867
0.85	0.10	512	6800	524288	0.300	50	2.32189
0.85	0.10	1024	2500	2097152	0.300	50	2.30592

Chapter 5

3-spin model as candidate for structural glass physics

5.1 Introduction

Our knowledge of the glassy state is remarkably limited when considering its prevalence in nature and modern materials. Silica is the most abundant mineral in the Earth's crust, and is found in amorphous form as window glass and optical fibers. LCD displays and thin-film photovoltaics utilize amorphous silicon, and the majority of plastics are amorphous as well. Despite our familiarity with and need for glassy materials, we yet lack a theoretical description of the glass transition. Experiments near this transition are naturally difficult to perform because of the slow dynamics. In order to approach the problem from a different angle, we can turn to the study of spin glasses and attempt to find models that make good analogies for structural glasses. The

similar topological description of the free energy surfaces suggest there is a connection between the two. And, since spin glasses tend to be simpler to simulate, there is strong interest in this type of investigation. So far, the best candidates seem to be the Potts glasses with more than four states [16, 27, 45, 8] , and "p-spin" models where interactions occur between $p > 2$ spins [44, 43].

The strongest established connection between these spin models and structural glass physics lies in the equations of mode coupling theory(MCT) [24]. MCT successfully captures the high-temperature dynamics of glass formers, including the region between the melting and glass transition temperatures, $T_G < T < T_M$. Remarkably, the MCT equations appear exactly in the dynamical mean field theory of the p-spin and Potts glasses. More specifically, it is the original, "idealized" MCT that matches these models, which predicts a dynamical arrest at T_D, a temperature greater than T_G. The spin models likewise feature a dynamical transition at T_D above a thermodynamic transition at T_C. Such an arrest, with a divergent relaxation time, does not occur in nature and represents the theory's failure to incorporate "activated processes" which allow the system to move between free energy valleys. A later modification to the theory addresses this [25]. This arrest occurs in the spin glass MFTs for the same reason: infinite dimensionality bars droplets from forming, meaning no activated processes.

While the dynamical transition is unphysical, there is some speculation that the static transition may correspond to an *ideal* glass state. This proposal arises from what has been termed an *entropy crisis* in supercooled liquids. Above the melting temperature, the liquid state has an amount of entropy ΔS_f more than the crystalline

state– the entropy of fusion. In general, liquids feature a higher heat capacity than the corresponding crystal, which means if the system is sufficiently cooled *as a liquid*, the entropy of the two states will match at a temperature T_K, called the Kauzmann temperature [42]. Questions about conflicts with the 3rd law of thermodynamics then arise. In practice, the glass transition occurs before T_K is reached, which takes the supercooled liquid out of equilibrium. It has been suggested that the glass transition is then driven by the existence of a thermodynamic transition at T_K corresponding to an amorphous ground state i.e. the ideal glass. Such an idea can reasonably be linked to the T_C found in the spin glass mean field theories.

The thermodynamic transition in the p-spin MFT is of a different character than standard replica symmetry breaking (RSB) transitions. The RSB-type solution found for the Sherrington-Kirkpatrick (SK) model [63, 64, 65] is termed *full* RSB, in that below T_C there exist an infinite number of pure states which show up in the continuous Parisi order parameter $q(x)$. For p-spin models, a different solution called one-step RSB or "1RSB" appears [21], characterized by a step-function order parameter– the symmetry is only broken once so there are only two values of the overlap, $q = 0$ and $q = q_1$. Furthermore, the value q_1 jumps discontinously at the critical temperature, leading some to call the transition "quasi-first order". This 1RSB-type transition of p-spin glasses has been connected with the ideal glass transition [58].

Presently, the goal is to stretch this analogy beyond that of mean field theory, to systems of realistic dimension. In the ideal scenario, the commonalities between structural and spin glasses present at mean-field level will hold, while changes such as

the merging of the separate dynamical singularity with the static transition will occur. Earlier work [52] found a second-order phase transition in a 4D 3-spin model. A second study [1], on a 4-spin model in 3D claimed to be near the lower critical dimension, with weak evidence for a transition. However, using even p maintains time-reversal symmetry while odd p destroys it. Such motivation led Moore and Drossel [57] to study, and ultimately find, a connection between the 3-spin glass and the Ising glass in a field. They propose that they are in the same universality class, which means our recent results for the latter model [38] provide further context (see Chapter 4).

5.2 Model and Methodology

Since the goal is to examine how well the mean field theory behavior of a p-spin glass model carries into dimensions below the upper critical dimension, we have an interest in probing multiple dimensions. As detailed in section 4.2, this can be done well with a 1-D model with tunable long-range interactions. As before, the tunability is present in the *dilution probability* not the magnitude of the interaction. Instead of long-range bonds being weaker, they are less likely to be present. For the p-spin case, we simply add an extra spin at each site of the 1-D ring and then place interactions on each combination of 3 spins from the 4 spins available between two sites. The resulting Hamiltonian looks like,

$$\mathcal{H} = -\sum_{i,j} \varepsilon_{ij} \left(J_{ij}^{(1)} S_i S_j T_i + J_{ij}^{(2)} S_i S_j T_j + J_{ij}^{(3)} S_i T_i T_j + J_{ij}^{(4)} S_j T_i T_j \right) , \qquad (5.1)$$

where $S_i, T_i = \pm 1$ are the Ising spins at site i, the sum is taken over all pairs of *sites* i, j, and the interactions J_{ij} are Gaussian random numbers with zero mean and unit standard deviation. The dilution matrix is the same as in section 4.2–note that it will dilute all of the four site-to-site interactions here. There are again two intervals of interest: for $1/2 < \sigma \leq 2/3$ the model should exhibit mean-field behavior, and $2/3 < \sigma \leq 1$ corresponds to dimensionalities between the critical dimensions, $d_l = 2$ and $d_u = 6$ such that $2 \leq d < 6$.

To find evidence for transitions, we compute the two-point finite-size correlation length [62, 3, 74]. For our 3-spin model the wave-vector-dependent spin-glass susceptibility appears as

$$\chi_{\rm SG}(k) = \frac{1}{4L} \sum_{S,T} \sum_{i,j} \left[\Big(\langle \{S,T\}_i \{S,T\}_j \rangle_T - \langle \{S,T\}_i \rangle_T \langle \{S,T\}_j \rangle_T \Big)^2 \right]_{\rm av} e^{ik\,(i-j)}. \quad (5.2)$$

The summation over "S,T" implies adding up terms for each choice between the S_i and T_i spins where such a choice is denoted by "$\{S,T\}_i$". The correlation length is then given by [41]

$$\xi_L = \frac{1}{2\sin(k_{\rm m}/2)} \left[\frac{\chi_{\rm SG}(0)}{\chi_{\rm SG}(\mathbf{k}_{\rm m})} - 1 \right]^{1/(2\sigma-1)}, \quad (5.3)$$

where $k_{\rm m} = 2\pi/L$ is the smallest non-zero wave-vector compatible with the boundary conditions. The finite-size scaling form is the same as in Eq.(4.6),

$$\begin{aligned} &\xi_L/L \sim \mathcal{X}[L^{1/\nu}(T - T_c)]\,, \qquad \sigma > 2/3 \\ &\xi_L/L^{\nu/3} \sim \mathcal{X}[L^{1/3}(T - T_c)]\,, \quad 1/2 < \sigma \leq 2/3, \end{aligned} \quad (5.4)$$

with $\nu = 1/(2\sigma - 1)$ in the mean-field regime.

The equilibration test mentioned in 3.3 is used here in the form,

$$U(\hat{q}_l, q) = -\frac{1}{T}\left[\frac{N_b}{L}(1-\hat{q}_l)\right]_{\rm av}, \tag{5.5}$$

where $q = L^{-1}\sum_i[\langle S_i\rangle_T^2]_{\rm av}$ is the spin overlap, $\hat{q}_l = N_b^{-1}\sum_{i,j}\varepsilon_{ij}\langle S_iS_j\rangle_T^2$ is the link overlap of a given sample, and N_b is the number of nonzero bonds of the sample. In these expressions, the S_i can be either spin at a site, written as S_i and T_i in the Hamiltonian. Because we need to compute the "connected" correlation function in Eq. (5.2) we simulate *four* replicas for each temperature. To speed up equilibration we use the exchange Monte Carlo method [23, 30]. For details on the simulation parameters see Table 5.1.

5.3 Results

The first results presented are for the case of $\sigma = 0.55$, shown in Fig. 5.1. This is data based on the correlation length against the temperature, which provides evidence for a transition through the crossing of data sets from different sizes. As this value of σ is well within the mean-field regime, we must change the finite-size scaling form as in Eq.(5.4). Thus we use $\xi_L/L^{10/3}$ which causes the data to cross at temperature values $T \simeq 2$. We note some variation in the crossing points, so these are plotted in Fig. 5.3 to clarify this behavior. Although $\sigma = 0.6$ was studied instead in Chapter 4, it is expected to behave qualitatively the same as $\sigma = 0.55$. Thus, there is an agreement between the models on finding a transition in the mean field region.

Next we show results for $\sigma = 0.75$ in Fig. 5.2. Finite-size effects are apparent

for small sizes, but the larger sizes seem to converge towards a common intersection. This analysis was done in detail and is displayed in Fig.5.3 alongside results for $\sigma = 0.55$. The data for a given size were fit to a cubic spline and the intersection of these splines for consecutive sizes $\{L, 2L\}$ was calculated. In order to estimate the error bars, we performed a bootstrap resampling. Fitting these points to a form $T_{cross}(\{L, 2L\}) = T_\infty + AL^{-\omega}$ gives a non-zero asymptotic value which should correspond to T_C. The fit parameters suggest $T_C = 1.13(5)$ and $\omega = 0.73(10)$. Here we find a disagreement with the $\sigma = 0.75$ data from Chapter 5 (see Fig.4.5). We note, however, that the data *do* agree with the results from Ref [51], which uses a different analysis method (and a slightly different model). See Chapter 4 for details on how this analysis differs.

We mention two other considerations on the disagreement for $\sigma = 0.75$. First, the 3-spin model maps to an Ising model with some field strength h_{3sp}. This value hasn't been derived, but M. A. Moore has suggested (private communication) that this field is small. Thus, it is possible that h_{3sp} is different enough from $h = 0.1$ to make the present comparison fail in some cases. Another scenario is that the correlation length for the p-spin model experiences sharp growth around an apparent T_C but eventually saturates to a large, finite value. This defines a length scale L_*: simulations performed at $L < L_*$ will find false evidence for a transition. This was shown for three dimensions within the Migdal-Kadanoff approximation [57]. It is feasible that at $\sigma = 0.75$ L_* is rather large and we are not simulating systems of sufficient size.

Lastly, Fig. 5.4 contains the data for $\sigma = 0.85$, roughly $d \sim 3$. Again, finite-size effects appear as the small sizes show crossings but the larger sizes begin to separate,

notably $L = 256$. These data suggest the lack of a transition, which is now in agreement again with the Ising model in a field (see Fig.4.5). It would appear the 3-spin model has a lower critical dimension in the rough vicinity of three or four given the results for $\sigma = 0.75$.

5.4 Summary

We have looked for evidence of 2nd-order transitions using a long-range one-dimensional 3-spin Ising spin-glass model. We find transitions in both the mean field and non-mean-field regions suggesting a "lower" critical value $\sigma_l > 0.75$. This disagrees with the data for the Ising spin-glass in a field, where transitions only occured for $d > 6$ (mean field, $\sigma < 2/3$) [38] as seen in Chapter 4. Possible complications involve a large, non-divergent correlation length for $d < 6$ that gives false evidence of a transition for our $\sigma = 0.75$ data. This scenario is supported by the Migdal-Kadanoff approximations performed by Moore and Drossel [57]. Also, the 3-spin model may map to a Ising model with a field h_{3sp} significantly different than $h = 0.1$, which could stretch the comparison in some cases.

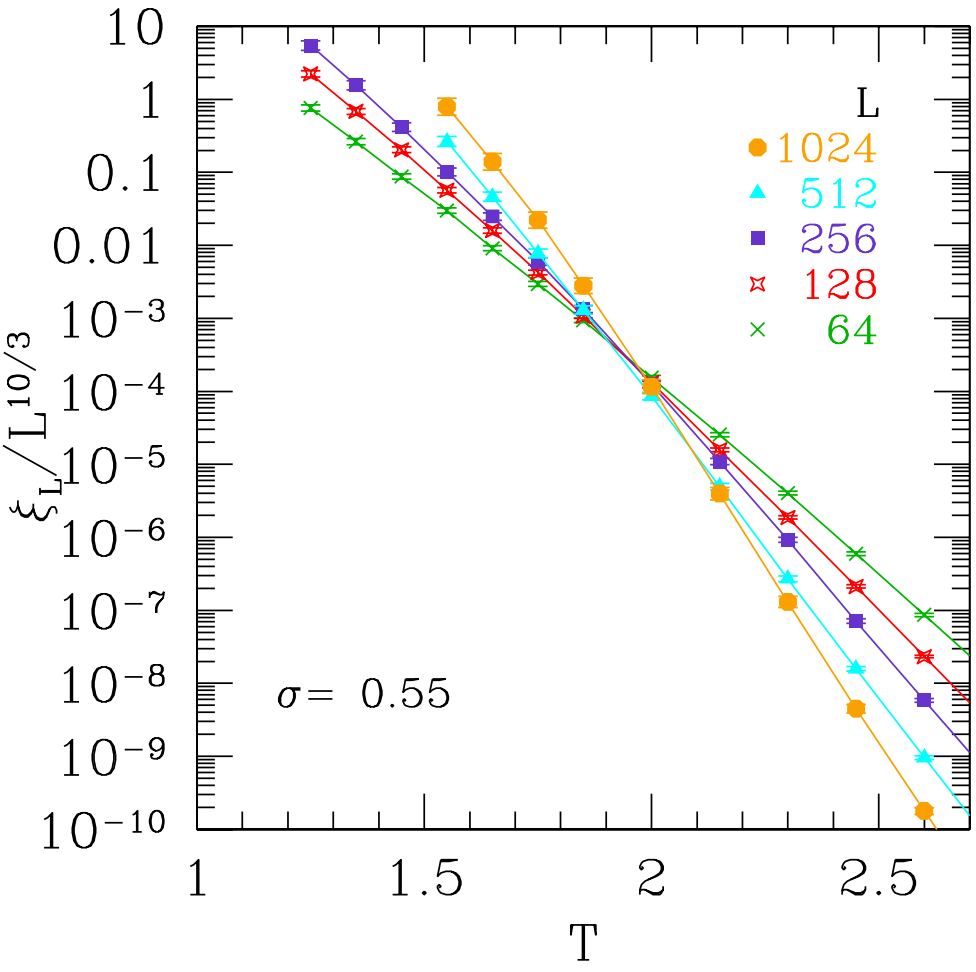

Figure 5.1: Finite-size correlation length divided by $L^{\nu/3}$ $(= L^{10/3})$ as a function of T for different sizes for $\sigma = 0.55$ (mean field region).

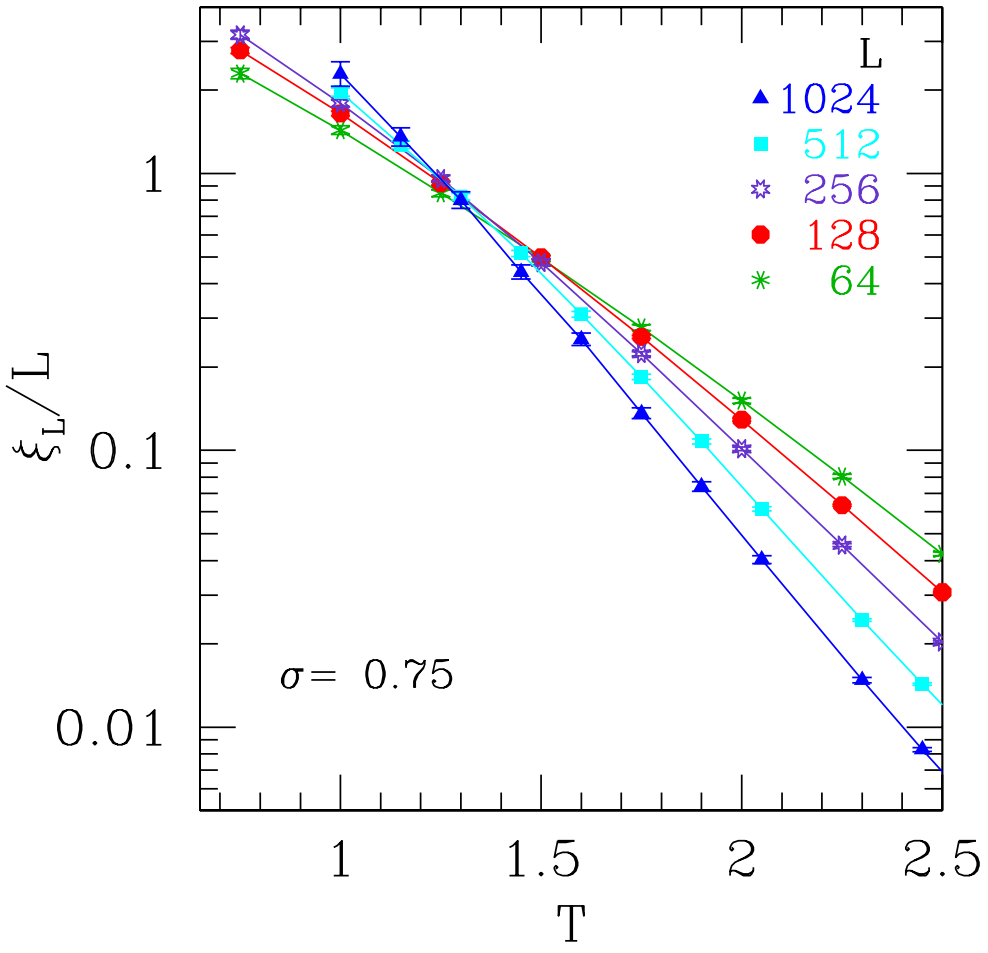

Figure 5.2: Similar to Fig.(5.1) but with $\sigma = 0.75$ and the non-mean-field form of scaling ξ/L. Again the data cross, though with larger corrections to scaling.

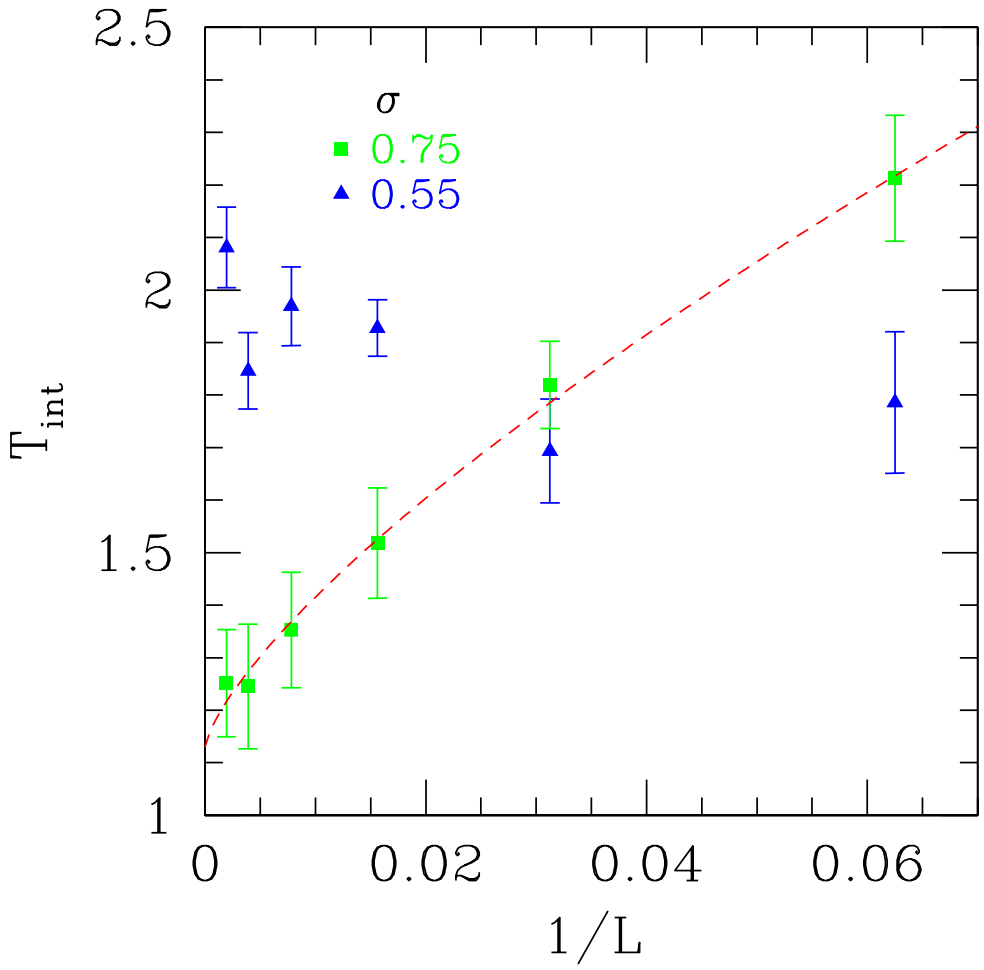

Figure 5.3: Analysis of the intersections between dimensionless correlation length curves for consecutive system sizes $\{L, 2L\}$. Fit to a form $T_{cross}(\{L, 2L\}) = T_\infty + AL^{-\omega}$ shown by the dashed line.

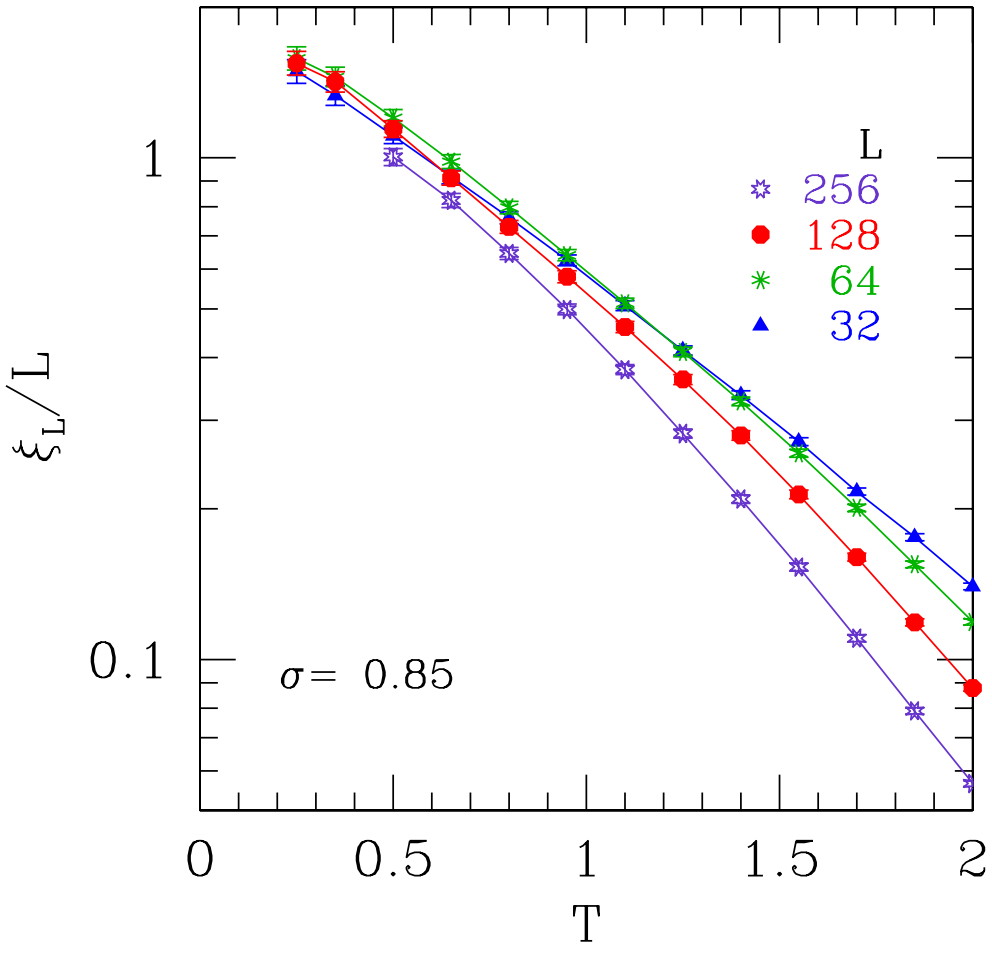

Figure 5.4: Lowering the effective d further with $\sigma = 0.85$ causes the transition to vanish. With size $L = 256$ there is a clear lack of ordering at low temperatures.

Table 5.1: Parameters of the simulations for different exponents σ. $N_{\rm sa}$ is the number of samples, $N_{\rm sw}$ is the total number of Monte Carlo sweeps, $T_{\rm min}$ is the lowest temperature simulated, and N_T is the number of temperatures used in the parallel tempering method for each system size L. The last column shows the parameter A [Eq. (4.2)] fixing $z_{\rm av} = 6$ neighbors.

σ	L	$N_{\rm sa}$	$N_{\rm sw}$	$T_{\rm min}$	N_T	A
0.55	64	10000	65536	1.250	16	0.95527
0.55	128	10500	131072	1.250	16	0.81746
0.55	256	4400	524288	1.250	16	0.72314
0.55	512	3150	1048576	1.550	13	0.65411
0.55	1024	850	2097152	1.550	13	0.60129
0.75	32	5000	65536	0.750	11	2.02742
0.75	64	5000	131072	0.750	11	1.82345
0.75	128	16300	524288	0.750	11	1.71141
0.75	256	8500	2097152	0.750	11	1.64289
0.75	512	5600	16777216	1.000	15	1.59859
0.75	1024	1000	33554432	1.000	15	1.56903
0.85	32	5000	65536	0.250	23	2.65088
0.85	64	5000	262144	0.250	23	2.47900
0.85	128	4750	4194304	0.250	23	2.39485
0.85	256	3800	16777216	0.500	21	2.34867

Chapter 6

Griffiths phase in 2D XY diluted ferromagnet

6.1 Introduction

When simulating disordered systems, one is generally first interested in the macroscopic behavior. One generally finds this by simulating many different *realizations* of the disorder, and averaging these results. With sufficient statistics and careful analysis, good estimates for the thermodynamic limit can be reached. Often, there exists even deeper physics that require knowledge of the *distributions* of observables as a function of some system parameter, such as the source of disorder. Theories that explain macroscopic phenomena may predict a specific distribution for some such observable. Also, it may occur that certain rare events, lying in the tail of these distributions, contribute significantly to the observed behavior.

This is the case for the Griffiths singularity, which was predicted for diluted ferromagnetic systems [26]. For example, the Ising ferromagnet in two dimensions has the well- known transition temperature $T_C(p = 1) \simeq 2.269$. Diluting this system (by removing either sites or bonds) will reduce T_C until the it reaches zero at the percolation limit, $T_C(p = 0.5) = 0$. For a dilution $0.5 < p < 1.0$, it was shown that a fully connected cluster of size L, in which all of the bonds are present, has a probability of appearing that decays as an exponential in L. This cluster is essentially an undiluted subsystem which will change behavior at $T = T_C(p = 1)$. As a result, the diluted system behaves differently below the transition temperature for the pure system. This is called the "Griffiths Phase", occuring between $T_C(p)$ and $T_C(p = 1)$ for all $0 \leq p < 1$. There is negligible change in the average susceptibility due to the Griffiths Phase, but the tail of the susceptibility distribution should show exponential behavior. Indeed, a prior study, upon which the present work is based, found evidence for this behavior [29].

Whether such an investigation will meet with success for a different type of diluted ferromagnet, one with XY spins, is addressed. The undiluted ($p = 1$) model has been studied extensively, and is the primary example of a system that undergoes a Kosterlitz-Thouless transition [48] at a critical temperature $T_C \simeq 0.895$. Below this temperature, a "Quasi Long-Range Ordered" (QLRO) phase exists. As seen in the Ising case, diluting the XY ferromagnet will lower the critical temperature until the percolation threshold is reached, where the transition disappears. It is predicted that the Griffiths phase will exist between the undiluted and diluted transition temperatures, as in the Ising case.

6.2 Method for probing tails of distributions

The naive way to measure the probability distribution of an observable would be to simply perform M simulations and bin the results into a histogram. This is termed "simple sampling" and one is unable to probe any deeper than a probability of $p = \frac{1}{M}$. This is insufficient to probe the tails of the susceptibility distribution. This situation echoes the sentiment expressed in Section 2.1 where an importance sampling method was derived for Monte Carlo. A similar technique can be used in the present context, by considering a different observable than energy.

However, in the previous case we knew the distribution we were trying to achieve–the Boltzmann distribution. Here, the distribution is unknown and is the item of interest. It may seem paradoxical at first, attempting to use an unknown distribution to guide the simulation, but the key is that the distribution is only unknown before the simulation begins. As one begins to gather statistics, a rough approximation can be made. This approximation, which we will term the *guiding function*, can then be used to drive the simulation to explore the tails of the distribution [47]. These new statistics can be used to further enhance the approximation and better guide the simulation. Ideally, the statistical information is fed back into the distribution approximation as soon as it is gathered. In this way, much less time is spent on simulating common outcomes so a better estimate for the rare events can be achieved. Such an implementation is detailed below, which follows the prescription given in Ref.[29]. The method can be applied for any given observable Q, which is how it will be presented. In this study, Q will be the

susceptibility.

We begin with a flat initial distribution for the guiding function, $G(\langle Q \rangle) = 1$, which is discretized into a fixed number of weights. Also, we have a modification factor C, set to some initial value $C > 1$, and the number of samples set to $N = N_0$. Then, perform a single simulation measuring the observable $\langle Q \rangle$ using a set of bonds $J^{(0)}$ drawn from the distribution $P(J)$. After this, begin the following

1. Perform the following loop for N iterations

   (a) Generate a candidate set of bonds J' by replacing a small fraction of them with new bonds drawn from $P(J)$. A fraction of 5 percent was found to be reasonable and used in the present study.

   (b) Measure $\langle Q \rangle$ for the bonds J'. This will be done by a Monte Carlo simulation.

   (c) Accept the candidate set of bonds J' with probability,

   $$P_{accept} = min\Big[\frac{G(\langle Q \rangle(J^{(i)}))}{G(\langle Q \rangle(J'))}, 1\Big] \tag{6.1}$$

   where $G(\langle Q \rangle(J^i))$ represents the value of the guiding function at the value $\langle Q \rangle$ measured for the previous set of bonds $J^{(i)}$. This favors a move away from sets of bonds that give common values for $\langle Q \rangle$ and towards rare values. If accepted, $J^{(i+1)} = J'$, otherwise $J^{(i+1)} = J^{(i)}$ (keep the old value).

   (d) Multiply the appropriate weight of $G(\langle Q \rangle)$ by C: $G(\langle Q \rangle(J^{(i+1)})) \rightarrow C \cdot G(\langle Q \rangle(J^{(i+1)}))$.

2. Normalize $G(\langle Q \rangle)$ by making sure the sum of the weights equals one.

3. Increase the number of samples to run, $N \rightarrow 2N$.

4. Reduce the value of C by $C \rightarrow \sqrt{C}$. Stop if C is less than some cutoff, otherwise return to step 1.

When finished with the simulation, $G(\langle Q \rangle)$ will be a good approximation of the actual probability $P(\langle Q \rangle)$.

6.3 Model and Observables

The model under consideration is the 2D bond-diluted XY ferromagnet. As the spins are represented by vectors residing in a common plane, there is a single, continuous degree of freedom (planar angle) for each. The Hamiltonian can be written as the following,

$$\mathcal{H} = -\sum_{\langle i,j \rangle} J_{ij} S_i \cdot S_j \tag{6.2}$$

where the bond dilution appears in the J_{ij} term as $P(J_{ij}) = p\delta(J_{ij} - J) + (1-p)\delta(J_{ij})$ and the summation is over nearest neighbors.

As this is an unfrustrated model, a cluster algorithm can be easily applied to efficiently simulate the system through the critical region. I used the Wolff algorithm [73] as it is a straightforward implementation. The simulations were performed for a length of time sufficient to achieve stationarity. Initially, the constant C used to modify the guiding function was set to $e = 2.718\cdots$ and the simulation was halted after it reached $C < 1.0001$ yielding 13 iterations. Full details of the simulational parameters can be found in Table. (6.1).

We are looking for evidence of the Griffiths singularity by analyzing the tail of the magnetic susceptibility distribution. In order to calculate the susceptibility for an XY system, one can simply look at one cartesian component of the spins,

$$\chi = \frac{1}{N}\Big\langle \Big(\sum_i S_i \cdot \hat{x} \Big)^2 \Big\rangle. \tag{6.3}$$

For a bond density $0.5 < p < 1.0$ we would expect to see three different types of behavior while moving from $T = 0$ to $T > T_{KT}$, as such a vertical line drawn on the phase diagram shown in Fig.(6.1) would enter each phase. First, $p = 0.85$ is studied to find the boundary between the QLRO and Griffiths phase. This choice of p is such that $T_C(p)$ is not too low, allowing shorter simulation times. Then, in order to examine the transition between the Griffiths and paramagnetic phases, a bond density of $p = 0.6$ seemed a good choice. This pushes the QLRO phase to low-temperature, so it will not to interfere, while maintaining a reasonably large p–one would expect the signature of the Griffiths phase to diminish as p decreases.

6.4 Results

We begin with the data for $p = 0.85$, showing the sets across size for $T = 0.50$ in Fig.(6.2). For sizes $L = 12, 24$, one can see the accuracy threshold for those particular simulations by noting how the data flatten out on the edges. Data for temperatures up to $T = 0.90$ were gathered, thus crossing $T_C(p = 0.85)$ as well as $T_C(p = 1)$. The analysis here is concerned only with the position of the peaks in the susceptibility distributions. These data are shown in Fig.(6.3). We expect these to follow the scaling

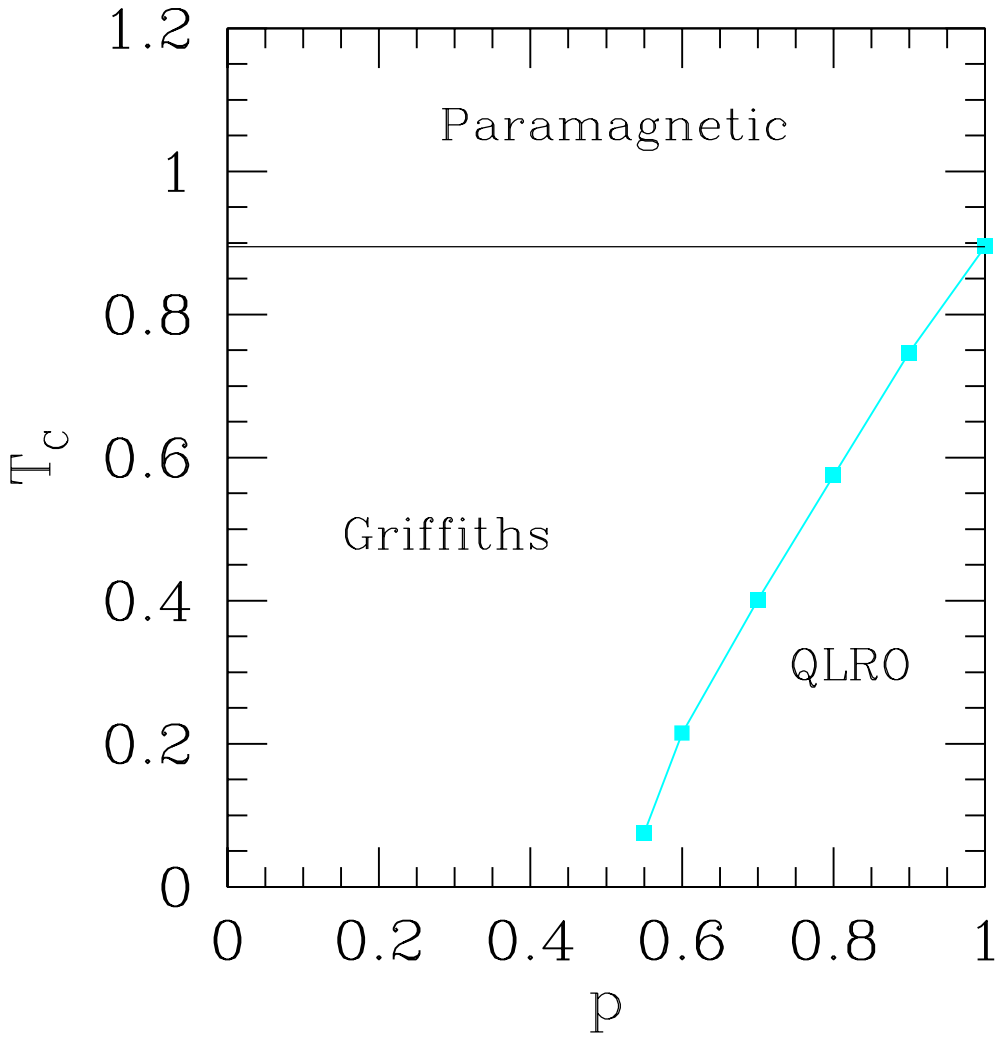

Figure 6.1: Phase diagram for the diluted XY ferromagnet [68, 29]. Below a high temperature paramagnetic phase, one finds quasi-long-range order (QLRO) if the bond density is sufficent. Otherwise, one expects a Griffiths phase with observable features in the dynamics and (weakly) in the statics.

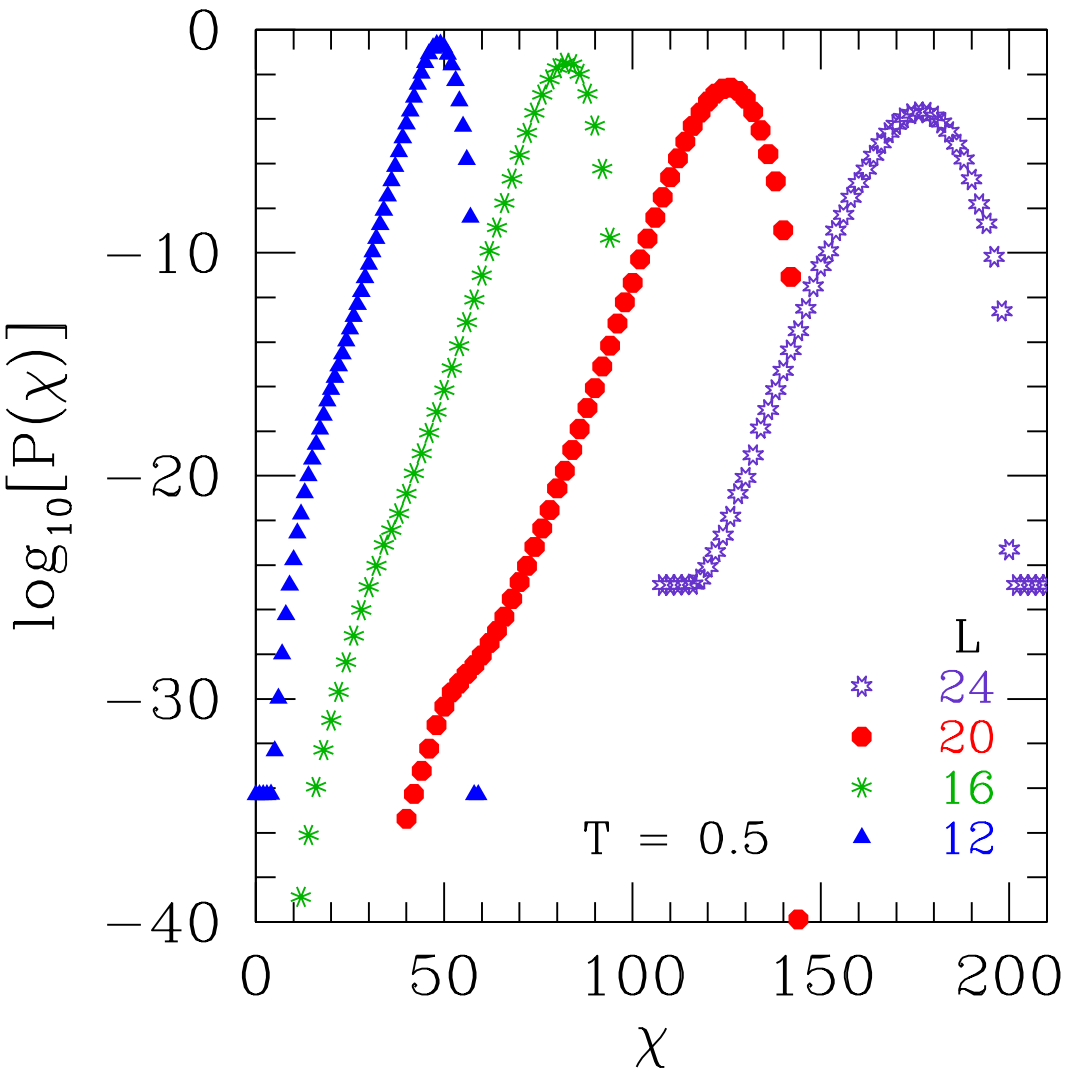

Figure 6.2: Distribution of the magnetic susceptibility for bond density $p = 0.85$ at a temperature $T = 0.5 < T_C(p)$. The analysis of these data uses the peak in the probability of χ.

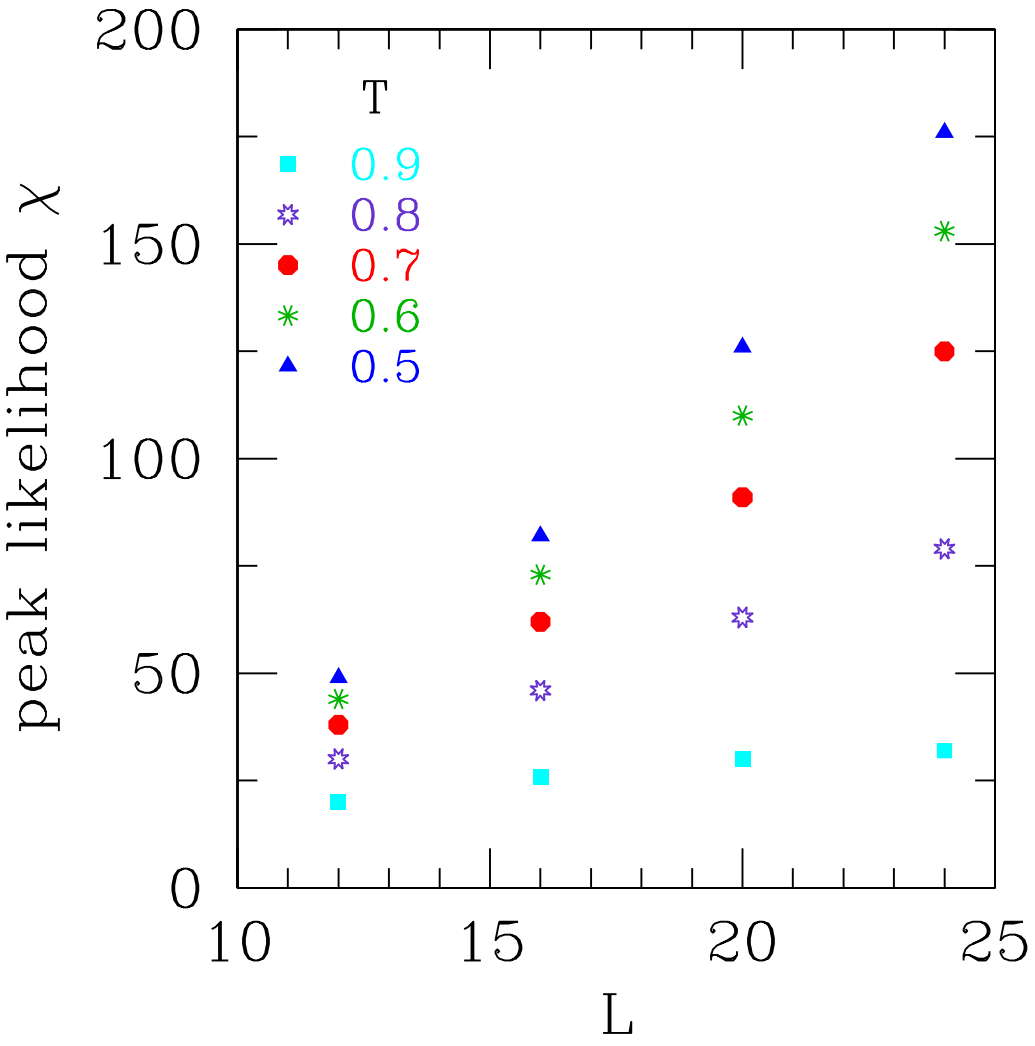

Figure 6.3: Plot of the peak position in the susceptibility distribution for all combinations of T and L. These data are fit to a power law, $\chi_{peak} \propto L^{2-\eta}$, to extract the exponent η.

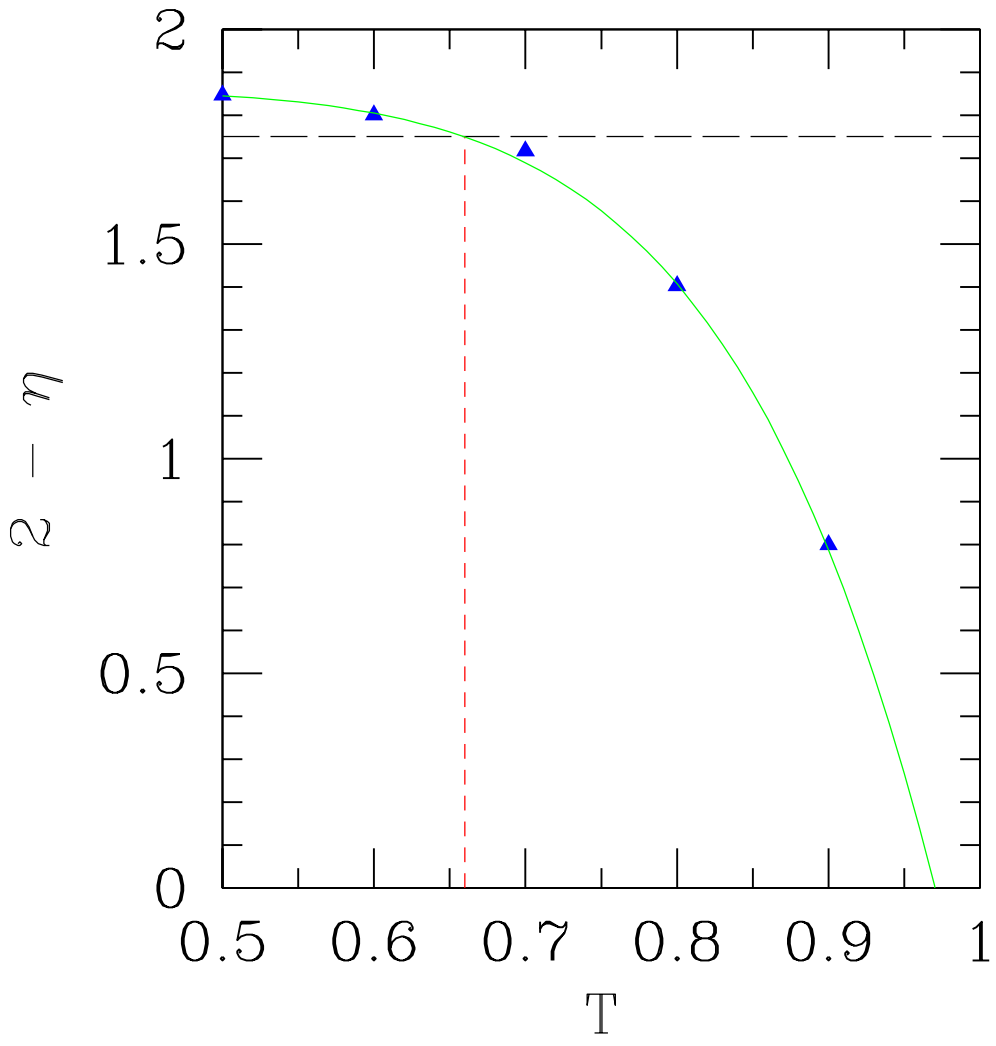

Figure 6.4: The data points are results from the fits of the data in Fig.(6.3). These have been fit to a functional form $(2-\eta) = A - B/L^C$ and the horizontal long-dashed line represents the theoretical value $\eta = 1/4$ at T_C. The intersection point gives $T_C \simeq 0.660$.

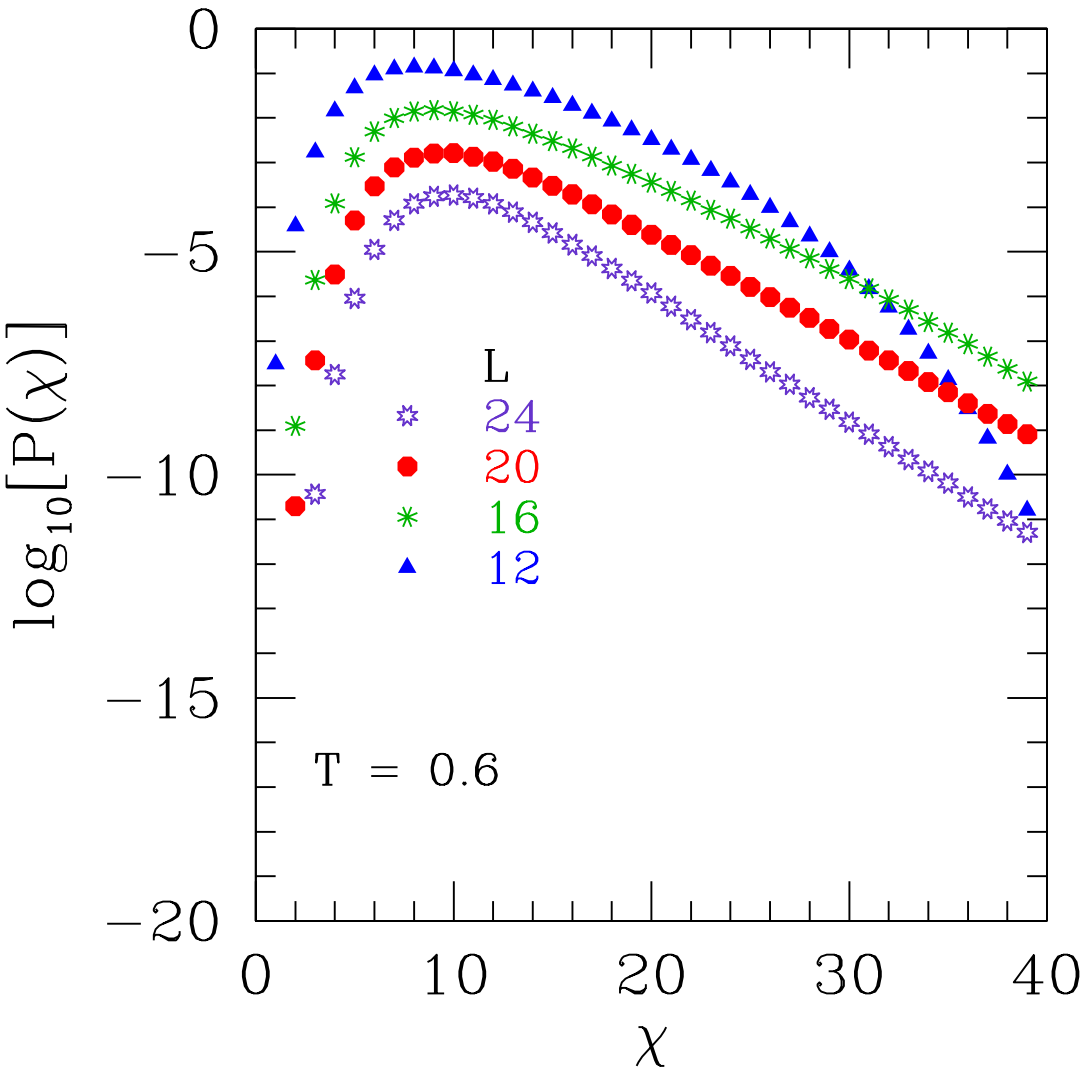

Figure 6.5: Distribution of the magnetic susceptibility for bond density $p = 0.60$ at a temperature $T = 0.5 > T_C(p)$. The data are shifted down by an amount proportional to L for easier viewing. Size $L = 12$ appears to be too small here while data in the high-χ tail for the larger sizes $L = 20, 24$ is well-fit by an exponential form.

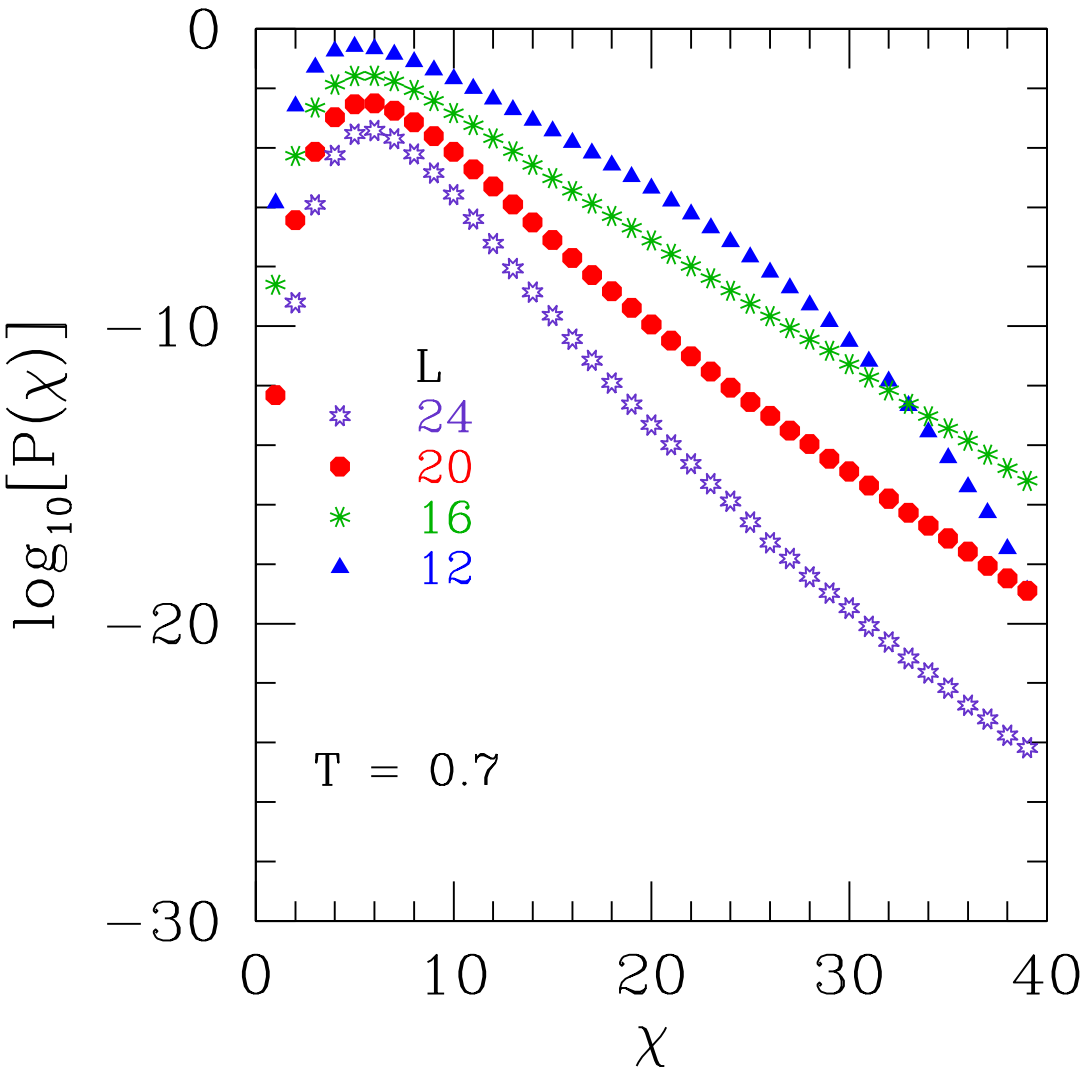

Figure 6.6: Same as Fig.(6.5) except $T = 0.7$. Note the slight upcurve in the tails of $L = 20, 24$.

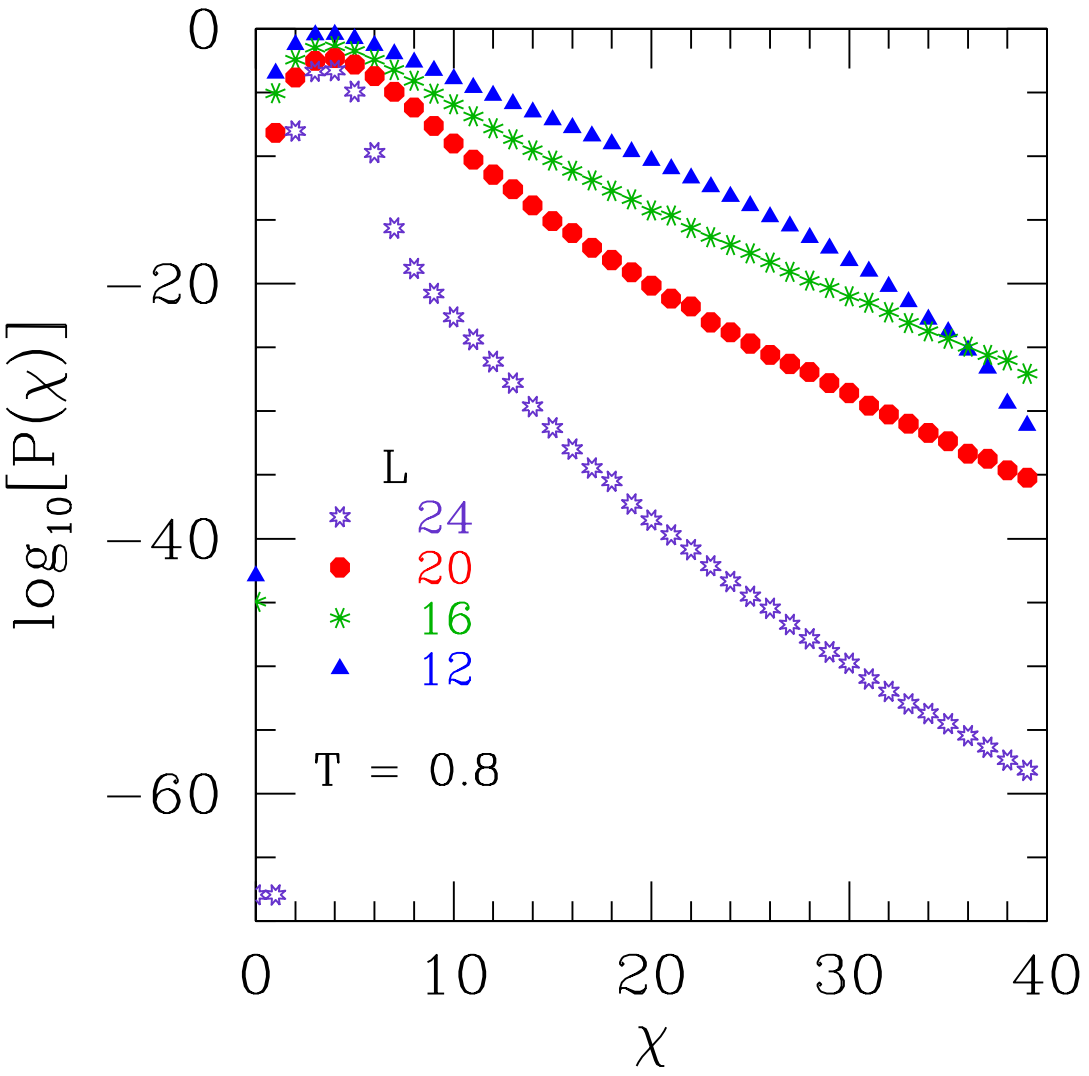

Figure 6.7: Same as Fig.(6.5) except $T = 0.8$. The curvature in the tail is more pronounced as it appears a strong peak is developing for low χ.

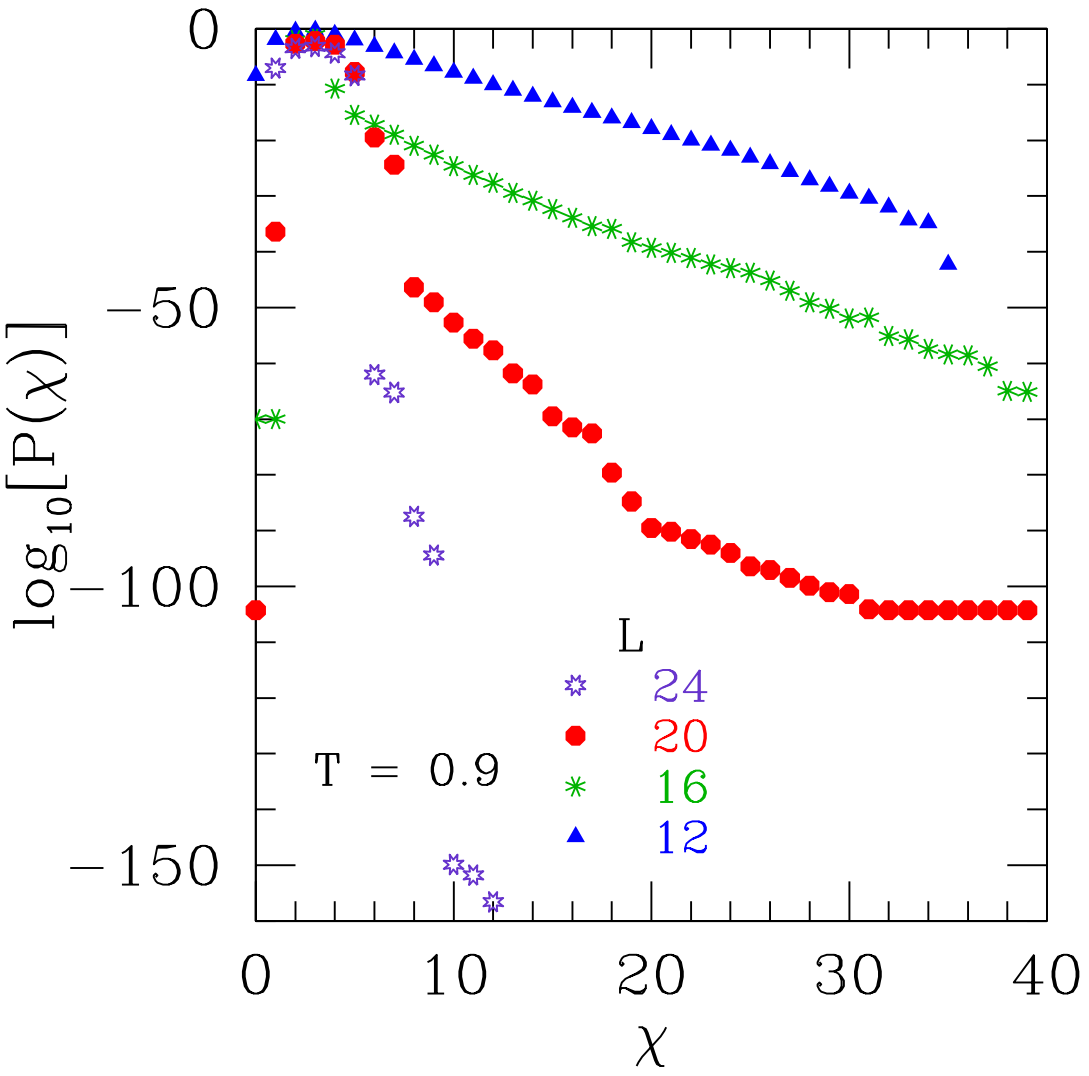

Figure 6.8: Same as Fig.(6.5) except $T = 0.9$. This is just above $T_C(p = 1) \simeq 0.895$. The long tail has been destroyed for sizes $L = 24$ and is quite weak for $L = 20$.

form $\chi_{peak} \propto L^{2-\eta}$ where η is a function of temperature and the theoretical value at T_C is $\eta(T_C) = 1/4$. After fitting these on a log-log scale, the slopes $(2 - \eta(T))$ are plotted in Fig.(6.4). These were then fit to a function $2 - \eta(T) = A - B/L^C$ (solid line) in order to extrapolate the temperature where $\eta(T) = 1/4$. This extrapolation is shown by the dashed lines. The resulting estimate is $T_C \simeq 0.660$ which compares favorably to an extrapolation from recent literature data [68], $T_C = 0.661(1)$.

The second four figures starting with Fig.(6.5) show the behavior of $p = 0.6$ as one increases the temperature to $T_C(p = 1)$. The first shows data at $T = 0.6$, where it seems $L = 12$ has finite-size effects causing it to round out. The other sizes have strong linear behavior that can be fit well to an exponential (the y-axis is plotted on a logarithmic scale). This is what we expect to see in the Griffiths phase. The next figure is similar, however $L = 12$ has straightened out a bit while $L = 16, 20$ now show signs of upward curvature. This effect is especially pronounced in Fig.(6.7) for $L = 24$. It appears that there are two competing features: a sharp peak at low χ and the exponential tail to large χ. As such, it is hard to extract a slope from the data tail, as the curvature is still present at $P(\chi) \sim 10^{-50}$. Lastly, Fig.(6.8) shows what happens as $T_C(p = 1)$ is crossed. $L = 20, 24$ show markedly changed behavior–any trace of the exponential tail is gone, down to extremely low probabilities. One can be certain that the Griffiths phase ceases to exist at or above this temperature.

To show rigorously that the Griffiths phase exists in the thermodynamic limit, one might extract the decay constants from the exponential fits for $T < 0.9$. Unfortunately, this analysis cannot be completed in a satisfactory manner. As the size of the

Table 6.1: Simulation parameters for 2D XY diluted ferromagnet

p	T	L	N_{sa}	N_{sw}	N_{bins}
0.60	$0.6, 0.7, 0.8, 0.9$	12	327660	1024	40
0.60	$0.6, 0.7, 0.8, 0.9$	16	327660	1024	40
0.60	$0.6, 0.7, 0.8, 0.9$	20	327660	2048	40
0.60	$0.6, 0.7, 0.8, 0.9$	24	327660	4096	40
0.85	$0.5, 0.6, 0.7, 0.8, 0.9$	12	327660	1024	40
0.85	$0.5, 0.6, 0.7, 0.8, 0.9$	16	327660	2024	60
0.85	$0.5, 0.6, 0.7, 0.8, 0.9$	20	327660	2024	80
0.85	$0.5, 0.6, 0.7, 0.8, 0.9$	24	163830	4024	100

simulation increases, either the tail phenomenologically gains curvature or near the peak it is influenced by the peak's behavior, giving it curvature that eventually vanishes. If the latter case is true, increasing the range and precision to which $P(\chi)$ is measured might yield some answers. Yet, is certainly possible that the tails are affected by other phenomena besides the Griffiths singularity, and only an analysis able to separate out the specific contributions of these would be successful here. Also, the "weaker" form of ordering present in XY models would reasonably cause the Griffiths-type behavior to show less strongly. As there appears to be no flaw in the theoretical argument for the Griffiths singularity, such arguments are more compelling than suggesting there is no Griffiths phase for $L \to \infty$.

6.5 Summary

Based on the results of this study, we can conclude that the distribution of the magnetic susceptibility properly responded to the QLRO phase— the peak in the distribution satisfied the expected scaling with system size. In fact, the agreement with prior values was surprisingly good [68], which suggests that methods such as those employed here may be useful in this type of investigation. In addition, an accurate estimate of the peak in these distributions takes considerably less computational effort than was expended here to analyze the distribution tails. However, it seems more effort is required to determine the full extent of the Griffiths phase in the XY model. There is strong evidence that above $T_C(p = 1)$ the Griffiths phase does not exist. Yet, its existence cannot be rigorously determined for the intermediate region. The data do suggest, qualitatively, that the Griffiths phase occurs in some capacity for $0.6 \leq T \leq 0.8$. For temperatures around $T = 0.6$ with bond density $p = 0.6$, long exponential tails would likely exist for reasonably large sizes, but extrapolating $L \to \infty$ is not possible with available data. Since the theoretical background is on solid footing, it would be most likely that the XY model is simply less influenced by the Griffiths singularity, compared to the Ising case, and it is much harder to detect as a result.

Chapter 7

Conclusion

7.1 Summary of Results

Our brief look into the optimization of parallel tempering for spin glasses suggested that there are no easy gains to be had with temperature set manipulation. The optimization technique performed well for the systems of higher symmetry in prior works, but the relative disorder of the EA glass washed out the features that allowed such improvements. It appears then that, for spin glasses, there is insignificant gain in temperature set optimization beyond what is already standard procedure.

We find in chapter 4 strong evidence against the existence of an AT line in finite dimensions, going against the replica symmetry breaking prediction and agreeing with the droplet picture. However, very recent results from another group have found that the method used to calculate xi_L/L suffers from finite size corrections that increase with field strength. It may therefore be a question of whether it as accurate enough

to detect a transition at the field strengths under study. If these are set too high, the error increases; too low and their effect will be smaller than is observable. Even so, this study represents the most extensive probe of the AT-line using well-established analytical techniques. While a complete description of the finite-dimensional spin glass phase is still lacking, the results suggests that RSB by itself will not provide such a description.

The study of the 3-spin model in Chapter 5 ties into the above results by a proposal that it belongs to the same universality class as the EA glass in a field. The difference in behavior at $\sigma = 0.75$ doesn't support this. If one considers the recent developments concerning the accuracy of xi_L/L analysis, however, there may be more to it. Regardless, it does seem unlikely that the mean field behavior will continue down to three dimensions, where the main interest lies. The p-spin model may still have use as a structural glass analogy in the mean field regime when treated specifically as a finite system [13] –no extrapolation to the thermodynamic limit. This is another way to regain the activated processes necessary to the picture, but absent in idealized MCT and infinite mean-field systems.

Chapter 6, somewhat of an aside, demonstrated the use of a very powerful technique for exploring deep into probability distributions. Some evidence for the Griffiths phase was found, yet the results were mixed. It might simply be the case that the Griffiths singularity is extraordinarily weak in XY models. The importance-sampling method applied to finding the distributions of observables performed extremely well, nonetheless. Undoubtedly, it can find application to a number of other areas.

Bibliography

[1] D. Alvarez, S. Franz, and F. Ritort. Fragile-glass behavior of a short-range p-spin model. *Phys. Rev. B*, 54:9756, 1996.

[2] P. W. Anderson and C. M. Pond. Anomalous dimensionalities in the spin-glass problem. *Phys. Rev. Lett.*, 40:903, 1978.

[3] H. G. Ballesteros, A. Cruz, L. A. Fernandez, V. Martin-Mayor, J. Pech, J. J. Ruiz-Lorenzo, A. Tarancon, P. Tellez, C. L. Ullod, and C. Ungil. Critical behavior of the three-dimensional Ising spin glass. *Phys. Rev. B*, 62:14237, 2000.

[4] J. R. Banavar and M. Cieplak. Nature of ordering in spin-glasses. *Phys. Rev. Lett.*, 48:832, 1982.

[5] U. Bengtzelius, W. Götze, and A. Sjölander. Dynamics of supercooled liquids and the glass transition. *J. Phys. C*, 17:5915, 1984.

[6] K. Binder and A. P. Young. Spin glasses: Experimental facts, theoretical concepts and open questions. *Rev. Mod. Phys.*, 58:801, 1986.

[7] S. Boettcher. Stiffness of the Edwards-Anderson Model in all Dimensions. *Phys. Rev. Lett.*, 95:197205, 2005.

[8] C. Brangian, W. Kob, and K. Binder. Evidence against a glass transition in the 10-state short-range Potts glass. *Europhys. Lett.*, 59:546–551, 2002.

[9] A. J. Bray and M. A. Moore. Some observations on the mean-field theory of spin glasses. *J. Phys. C*, 13:419, 1980.

[10] A. J. Bray and M. A. Moore. Lower critical dimension of Ising spin glasses: a numerical study. *J. Phys. C*, 17:L463, 1984.

[11] A. J. Bray and M. A. Moore. Scaling theory of the ordered phase of spin glasses. In L. Van Hemmen and I. Morgenstern, editors, *Heidelberg Colloquium on Glassy Dynamics and Optimization*, page 121. Springer, New York, 1986.

[12] Y. Cannella and J. A. Mydosh. Magnetic ordering in gold-iron alloys (susceptibility and thermopower studies). *Phys. Rev. B*, 6:4220, 1972.

[13] A. Crisanti and F. Ritort. Are mean-Field spin-glass models relevant for the structural glass transition? *Physica A*, 1-2:155–160, 2000.

[14] J. R. L. de Almeida and D. J. Thouless. Stability of the Sherrington-Kirkpatrick solution of a spin glass model. *J. Phys. A*, 11:983, 1978.

[15] S. F. Edwards and P. W. Anderson. Theory of spin glasses. *J. Phys. F: Met. Phys.*, 5:965, 1975.

[16] D. Elderfield and D. Sherrington. The curious case of the Potts spin glass. *J. Phys. C*, 16:L497, 1983.

[17] D. S. Fisher and D. A. Huse. Ordered phase of short-range Ising spin-glasses. *Phys. Rev. Lett.*, 56:1601, 1986.

[18] D. S. Fisher and D. A. Huse. Absence of many states in realistic spin glasses. *J. Phys. A*, 20:L1005, 1987.

[19] D. S. Fisher and D. A. Huse. Equilibrium behavior of the spin-glass ordered phase. *Phys. Rev. B*, 38:386, 1988.

[20] G. S. Fulcher. Analysis of recent measurements of the viscosity of glasses. *J. Am. Ceram. Soc.*, 8:339, 1925.

[21] E. Gardner. *Nucl. Phys. B*, 257:747, 1985.

[22] T. Geszti. Pre-vitrification by viscosity feedback. *J. Phys. C.*, 16:5805–5814, 1982.

[23] C. Geyer. Monte Carlo Maximum Likelihood for Depend Data. In *23rd Symposium on the Interface*, page 156, 1991.

[24] W. Götze. In J. P. Hansen, D. Levesque, and J. Zinn-Justin, editors, *Liquids, Freezing, and the Glass Transition*. North Holland, 1989. Les Houches session L1.

[25] W. Götze and L. Sjögren. The mode coupling theory of structural relaxations. *Transp. Theory Stat. Phys.*, 24:801, 1995.

[26] R. B. Griffiths. Nonanalytic behavior above the critical point in a random Ising ferromagnet. *Phys. Rev. Lett.*, 23:17, 1969.

[27] D. J. Gross, I. Kanter, and H. Sompolinsky. Mean-field theory of the Potts glass. *Phys. Rev. Lett.*, 55:304, 1985.

[28] M. Hasenbusch, A. Pelissetto, and E. Vicari. The critical behavior of 3D Ising glass models: universality and scaling corrections. *J. Stat. Mech.*, L02001, 2008.

[29] K. Hukushima and Y. Iba. A monte carlo algorithm for sampling rare events: application to a search for the griffiths singularity. arXiv:0711.0870v1, 2007.

[30] K. Hukushima and K. Nemoto. Exchange Monte Carlo method and application to spin glass simulations. *J. Phys. Soc. Jpn.*, 65:1604, 1996.

[31] D. A. Huse and D. S. Fisher. Pure states in spin glasses. *J. Phys. A*, 20:L997, 1987.

[32] E. Ising. *Z. Phys.*, 31:253, 1925.

[33] J. Jones and A. P. Young. Finite size scaling of the correlation length above the upper critical dimension. *Phys. Rev. B*, 71:174438, 2005.

[34] P. E. Jönsson, H. Takayama, H. Katori, and A. Ito. Absence of phase transition in a magnetic field in the $Fe_{0.55}Mn_{0.45}TiO_3$ Ising Spin Glass. *J. Mag. Mag. Mat.*, 310:1494, 2007.

[35] T. Jörg and F. Ricci-Tersenghi. Entropic Effects in the Very Low Temperature

Regime of Diluted Ising Spin Glasses with Discrete Couplings. *Phys. Rev. Lett.*, 100:177203, 2008.

[36] L. P. Kadanoff. Notes on Migdal's recursion formulas. *Annals of Physics*, 100:359, 1976.

[37] H. G. Katzgraber. Spin glasses and algorithm benchmarks: A one-dimensional view. *J. Phys.: Conf. Ser.*, 95:012004, 2008.

[38] H. G. Katzgraber, D. Larson, and A. P. Young. Study of the Almeida-Thouless line using power- law diluted one-dimensional Ising spin glasses. *Phys. Rev. Lett.*, 102:177205, 2009.

[39] H. G. Katzgraber, M. Palassini, and A. P. Young. Monte Carlo simulations of spin glasses at low temperatures. *Phys. Rev. B*, 63:184422, 2001.

[40] H. G. Katzgraber, S. Trebst, D. A. Huse, and M. Troyer. Feedback-optimized parallel tempering Monte Carlo. *J. Stat. Mech.*, P03018, 2006.

[41] H. G. Katzgraber and A. P. Young. Probing the Almeida-Thouless line away from the mean-field model. *Phys. Rev. B*, 72:184416, 2005. (Referrred to as KY).

[42] W. Kauzmann. The nature of the glassy state and the behavior of liquids at low temperatures. *Chem. Rev.*, 43:219–256, 1948.

[43] T. R. Kirkpatrick and D. Thirumalai. Dynamics of the structural glass transition and the p-spin-interaction spin glass model. *Phys. Rev. Lett.*, 58:2091, 1987.

[44] T. R. Kirkpatrick and D. Thirumalai. p-spin-interaction spin-glass models: Connections with the structural glass problem. *Phys. Rev. B*, 36:5388, 1987.

[45] T. R. Kirkpatrick and P. G. Wolynes. Stable and metastable states in mean-field Potts and structural glasses. *Phys. Rev. B*, 36:8552, 1987.

[46] A. Kone and D. A. Kofke. Selection of temperature intervals for parallel-tempering simulations. *J. Chem. Phys.*, 122:206101, 2005.

[47] M. Körner, H. G. Katzgraber, and A. K. Hartmann. Probing tails of energy distributions using importance-sampling in the disorder with a guiding function. *J. Stat. Mech.*, P04005, 2006.

[48] J. M. Kosterlitz and D. Thouless. Ordering, metastability, and phase transitions in two-dimensional systems. *J. Phys. C*, 6:1181, 1973.

[49] G. Kotliar, P. W. Anderson, and D. L. Stein. One-dimensional spin-glass model with long-range random interactions. *Phys. Rev. B*, 27:R602, 1983.

[50] L. Leuzzi, G. Parisi, F. Ricci-Tersenghi, and J. J. Ruiz-Lorenzo. Diluted One-Dimensional Spin Glasses with Power Law Decaying Interactions. *Phys. Rev. Lett.*, 101:107203, 2008.

[51] L. Leuzzi, G. Parisi, F. Ricci-Tersenghi, and J. J. Ruiz-Lorenzo. Ising spin glass transition in magnetic field out of mean-field. (arXiv-0811.3435), 2008.

[52] E. Marinari, C. Naitza, F. Zuliani, G. Parisi, M. Picco, and F. Ritort. General

Method to Determine Replica Symmetry Breaking Transitions. *Phys. Rev. Lett.*, 81:1698, 1998.

[53] E. Marinari and G. Parisi. Simulated tempering: A new Monte Carlo scheme. *Europhys. Lett.*, 19:451, 1992.

[54] E. Marinari, G. Parisi, and J. J. Ruiz-Lorenzo. On the phase structure of the 3d Edwards Anderson spin glass. *Phys. Rev. B*, 58:14852, 1998.

[55] W. L. McMillan. Scaling theory of Ising spin glasses. *J. Phys. A*, 17:3179, 1984.

[56] Alexander A. Migdal. Gauge Transitions in Gauge and Spin Lattice Systems. *Sov. Phys. JETP*, 42:743, 1975.

[57] M. A. Moore and B. Drossel. p-spin model in finite dimensions and its relation to structural glasses. *Phys. Rev. Lett.*, 89:217202, 2002.

[58] M. A. Moore and J. Yeo. The Thermodynamic Glass Transition in Finite Dimensions. *Phys. Rev. Lett.*, 96:095701, 2005.

[59] M. E. J. Newman and G. T. Barkema. *Monte Carlo Methods in Statistical Physics*. Oxford University Press Inc., New York, USA, 1999.

[60] R. Omari, J. J. Préjean, and J. Souletie. . *J. Phys. (Paris)*, 44:C9–1069, 1983.

[61] L. Onsager. *Phys. Rev.*, 117:1, 1944.

[62] M. Palassini and S. Caracciolo. Universal Finite-Size Scaling Functions in the 3D Ising Spin Glass. *Phys. Rev. Lett.*, 82:5128, 1999.

[63] G. Parisi. Infinite number of order parameters for spin-glasses. *Phys. Rev. Lett.*, 43:1754, 1979.

[64] G. Parisi. The order parameter for spin glasses: a function on the interval 0–1. *J. Phys. A*, 13:1101, 1980.

[65] G. Parisi. Order parameter for spin-glasses. *Phys. Rev. Lett.*, 50:1946, 1983.

[66] C. Predescu, M. Predescu, and C.V. Ciobanu. The incomplete beta function law for parallel tempering sampling of classical canonical systems. *J. Chem. Phys.*, 120:4119, 2004.

[67] D. Sherrington and S. Kirkpatrick. Solvable model of a spin glass. *Phys. Rev. Lett.*, 35:1792, 1975.

[68] T. Surungan and Y. Okabe. Kosterlitz-thouless transition in planar spin modes with bond dilution. *Phys. Rev. B*, 71:184438, 2005.

[69] G. Tammann and W. Hesse. Die abhängigkeit der viskosität von der temperatur bei unterkühlten flüssigkeiten. *Z. Anorg. Allg. Chem.*, 156:245–257, 1926.

[70] S. Trebst, D. A. Huse, and M. Troyer. Optimizing the ensemble for equilibration in broad-histogram Monte Carlo simulations. *Phys. Rev. E*, 70:046701, 2004.

[71] L. Viana and A. J. Bray. Phase diagrams for dilute spin glasses. *J. Phys. C*, 18:3037, 1985.

[72] H. Vogel. Das temperatur-abhängiglkeitsgesetz derviskosität von flüssigkeiten. *Phys. Zeit.*, 22:645–646, 1922.

[73] U. Wolff. Collective Monte Carlo updating for spin systems. *Phys. Rev. Lett.*, 62:361, 1989.

[74] A. P. Young and H. G. Katzgraber. Absence of an Almeida-Thouless line in Three-Dimensional Spin Glasses. *Phys. Rev. Lett.*, 93:207203, 2004.